From Pairwise Comparisons of Complex Behavior to an Overall Performance Rank: A Novel Alloy Design Strategy

Rafael Herschberg, Lisa Rateau, Laure Martinelli, Fanny Balbaud-Célérier, Jean Dhers, Anna Fraczkiewicz, Gérard Ramstein, Franck Tancret

metals

MDPI

Article

From Pairwise Comparisons of Complex Behavior to an Overall Performance Rank: A Novel Alloy Design Strategy

Rafael Herschberg [1], Lisa Rateau [1,2,3], Laure Martinelli [4], Fanny Balbaud-Célérier [4], Jean Dhers [3], Anna Fraczkiewicz [2], Gérard Ramstein [5] and Franck Tancret [1,*]

[1] Nantes Université, CNRS, Institut des Matériaux de Nantes Jean Rouxel, IMN, 44000 Nantes, France; rafael.herschberg@cnrs-imn.fr (R.H.); lisa.rateau@emse.fr (L.R.)
[2] MINES Saint-Etienne, Université de Lyon, CNRS, UMR 5307 LGF, Centre SMS, 42023 Saint-Etienne, France; fraczkie@emse.fr
[3] Framatome, 69006 Lyon, France; jean.dhers@newcleo.com
[4] CEA, Service de Recherche en Corrosion et Comportement des Matériaux, Université Paris-Saclay, 91191 Gif-sur-Yvette, France; laure.martinelli@cea.fr (L.M.); fanny.balbaud@cea.fr (F.B.-C.)
[5] Nantes Université, CNRS, Laboratoire des Sciences du Numérique de Nantes (LS2N), 44306 Nantes, France; gerard.ramstein@univ-nantes.fr
* Correspondence: franck.tancret@univ-nantes.fr

Abstract: A method is developed to exploit data on complex materials behaviors that are impossible to tackle by conventional machine learning tools. A pairwise comparison algorithm is used to assess a particular property among a group of different alloys tested simultaneously in identical conditions. Even though such characteristics can be evaluated differently across teams, if a series of the same alloys are analyzed among two or more studies, it is feasible to infer an overall ranking among materials. The obtained ranking is later fitted with respect to the alloy's composition by a Gaussian process. The predictive power of the method is demonstrated in the case of the resistance of metallic materials to molten salt corrosion and wear. In this case, the method is applied to the design of wear-resistant hard-facing alloys by also associating it with a combinatorial optimization of their composition by a multi-objective genetic algorithm. New alloys are selected and fabricated, and their experimental behavior is compared to that of concurrent materials. This generic method can therefore be applied to model other complex material properties—such as environmental resistance, contact properties, or processability—and to design alloys with improved performance.

Keywords: alloy design; machine learning; optimization; molten salt corrosion; wear

Citation: Herschberg, R.; Rateau, L.; Martinelli, L.; Balbaud-Célérier, F.; Dhers, J.; Fraczkiewicz, A.; Ramstein, G.; Tancret, F. From Pairwise Comparisons of Complex Behavior to an Overall Performance Rank: A Novel Alloy Design Strategy. *Metals* **2024**, *14*, 1412. https://doi.org/10.3390/met14121412

Academic Editor: Seyedmehdi Hosseini

Received: 29 October 2024
Revised: 29 November 2024
Accepted: 3 December 2024
Published: 10 December 2024

1. Introduction and Background

Historically, materials research has been made through trial and error, making it a very lengthy and costly procedure [1]. However, thanks to an explosion of the availability of experimental data coupled with advances in artificial intelligence, a new paradigm was born: materials informatics, which can improve and accelerate materials design and development [2]. For instance, regression by machine learning, e.g., using neural networks [3], Gaussian processes [4], support vector machines [5], or genetic programming [6], can be exploited to fit some characteristics of existing alloys as a function of composition and/or processing parameters and then to predict those of new materials in view of alloy design by combinatorial optimization [7]. Even though this approach has already been proven successful, there are still a few obstacles to address. First is the lack of databases large enough to cover the landscape of some specific properties, for which it is hard to make good predictions or where the machine learning algorithms might over fit the data [8,9]. Then since only a few selected data points are finally published in the scientific literature—where failed experimental results and abandoned projects never get to see the light of day—the final machine learning model does not consider all the possible data, making it biased [10].

Some promising advances have been made in hopes of solving this problem, such as the creation of centralized and highly specialized databases [11–13], while others have tried a holistic approach by coupling the automatization of experimental processing and characterization with modeling techniques [14,15], but such datasets remain largely inaccessible. In addition, certain complex material characteristics—like processability (e.g., castability, forgeability, weldability, etc.), environmental resistance (e.g., corrosion, hydrogen embrittlement, irradiation, etc.), or contact properties (e.g., friction, wear, etc.)—are not frequently assessed in a standardized fashion for a large variety of alloys, which results in a high experimental scatter across teams. Consequently, in such cases, no dataset exists or can even be assembled with a large amount of robust data collected in equivalent conditions to allow for a conventional machine learning treatment.

1.1. Structure of Comparative Data

The objective of this study is to present a strategy that tackles the above-mentioned obstacles, without the need for a centralized public database or an in-house experimental setup for data entry purposes through the exploitation of scarce and scattered pairwise comparative data. Indeed, it seems appealing and relevant to exploit data on the performance of materials that have been evaluated in identical conditions. Of course, each batch of experiments may have been implemented differently, but step by step and by proximity, a global rank may be inferred among all materials. An illustrative example is presented in Table 1 where, on each line, a comparison has been reported between two alloys previously tested in equal conditions in the case of corrosion experiments in molten salts.

Table 1. Pairwise comparison of alloys tested in identical experimental conditions in terms of the mass change of alloy *i* (Δm_i) relative to alloy *j* (Δm_j) during corrosion experiments in molten salts.

Ref.	Alloy *i*	Alloy *j*	Molten Salt	T (°C)	$\Delta m_i/\Delta m_j$
[16]	Hastelloy N	MoNiCr	FLiNaK	650	1.28
[17]	Inconel 625	Hastelloy N	Li_2BeF_4	750	1.45
[18]	Hastelloy C276	Inconel 625	NaCl-KCl-$MgCl_2$	700	1.57
[18]	SS316	Hastelloy C276	NaCl-KCl-$MgCl_2$	700	2.26
[19]	P91	SS316	$NaNO_3$-KNO_3	600	20.82

In this example, the first alloy *i* is worse than the second alloy *j*, assuming that a lower mass variation indicates better corrosion resistance by a measurable ratio $\Delta m_i/\Delta m_j$ (although this value is highly sensitive to the testing setup). From this simple example, the rank P91 > SS316 > Hastelloy C276 > Inconel 625 > Hastelloy N > MoNiCr can be easily inferred, where the symbol ">" means "worse than." If an arbitrary overall performance score S_1 is attributed to the best alloy (MoNiCr), it could also be possible to do the same for the others in Table 1 (where a higher score would reflect a worse performance), relying, for instance, on the relative weight variations. Hastelloy N would then have a score S_2, Inconel 625 a score S_3, and so forth until S_6 for P91, with $S_6 > S_5 > S_4 > S_3 > S_2 > S_1$.

Such a situation would be easy to implement without the need of a particular algorithm. Afterward, the rank, or the score, may be fitted as a function of alloy composition by a standard machine learning regression tool and used for material design, e.g., by combinatorial optimization. However, data on complex characteristics, such as processability, environmental resistance, or contact properties, are usually scattered and sensitive to experimental conditions so a situation such as in Table 1 is almost never found. Moreover, it may happen that, among a group of alloys (e.g., A, B, C, D, E, and F), the pairwise comparisons do not yield an obvious ranking (e.g., A > B, B > C, C > D, D > C, D > B, C > E, E > F, etc.). In such a scenario, even if a real overall hierarchy exists, it would be very arduous to assign ranks or scores manually, as in the previous example, especially if there is a vast amount of pairwise comparisons.

1.2. Envisioned Method

Such a task can be undertaken by specialized algorithms, called incomplete pairwise comparison algorithms, since they can establish a ranking among a set of objects when all available pairs have not been compared, which is usually the case in materials problems. The chosen algorithm is named SpringRank (SR), originally developed by De Bacco et al. [20] and intended to infer rankings of nodes in directed networks. It has been used, for instance, to model faculty hiring networks [21] and the ranking of American universities [22]. However, to the authors' knowledge, incomplete pairwise comparison algorithms have never been used as tools for materials design. The approach developed here, whose originality is the association of different tools within the specific context of alloy modeling and design, has several steps, which are reflected in the structure of the present publication. The first step is the use of a pairwise comparison algorithm to rank and score alloys according to their relative reported performance in complex situations. The second step consists in using a machine learning tool—a Gaussian process—to fit the obtained rank or score as a function of alloy composition so as to obtain a predictive tool of the relative alloy performance. The last step, when applied, is a multi-objective optimization of composition to design alloys with optimal performance. After a presentation of the method—pairwise comparison, machine learning, and optimization algorithms—it is applied to two different case studies—molten salt corrosion of structural alloys and wear resistance of hard-facing alloys (Works on the modeling and design of hard-facing alloys were performed between and 2019 and 2023 [23]; those on molten salt corrosion in 2023–2024 within projects ANR-22-PEXD-0003 and ANR-22-PEXD-0005)—from which trends solely based on chemical content can be identified. Lastly, the presented strategy will be validated by experimental results for the case of wear resistance.

2. General Method

2.1. Data Processing

Data processing also presented distinct steps that are common to each case study. Firstly, a database was built from publications available in the scientific literature, where at least two different alloys were tested in identical experimental conditions. Secondly, a list of alloys similar to Table 1 was built where alloy i had a worse performance than alloy j and its s_{ij} was calculated. (In the specific case of molten salt corrosion, s_{ij} was equal to $\Delta m_i / \Delta m_j$.) Lastly, the list of pairwise comparisons was fed into the SR algorithm in order to determine the rank of all alloys. The size of the database and its impact on the final result are discussed separately for each case study.

2.2. Pairwise Comparison Algorithm

A pairwise comparison algorithm starts with the basic assumption that all actors (i.e., alloys) are compared in a pairwise fashion and that there exists a hierarchical rank among them. This idea is used to describe the system as a directed network (see Figure 1 in the case of molten salt corrosion; data will be described later), where each individual i is a node and each pairwise comparison between objects i and j is a weighted and directed edge. The algorithm then builds an adjacency matrix A, where A_{ij} denotes the comparison between i and j individuals, where i is ranked above j with a given ratio s_{ij}. Then, SR models each edge as a physical spring and, by virtually stretching the network, finds the node's real-valued position that minimizes the total energy of the system, limiting inconsistencies in the ranking [24] and predicting pairwise comparisons from nodes that are not directly connected by an edge. Lastly, it provides an overall ranking of all actors by assigning them a score S_i. One of the main advantages of this algorithm is its computing efficiency: for both case studies, it took only a few seconds to predict an overall rank.

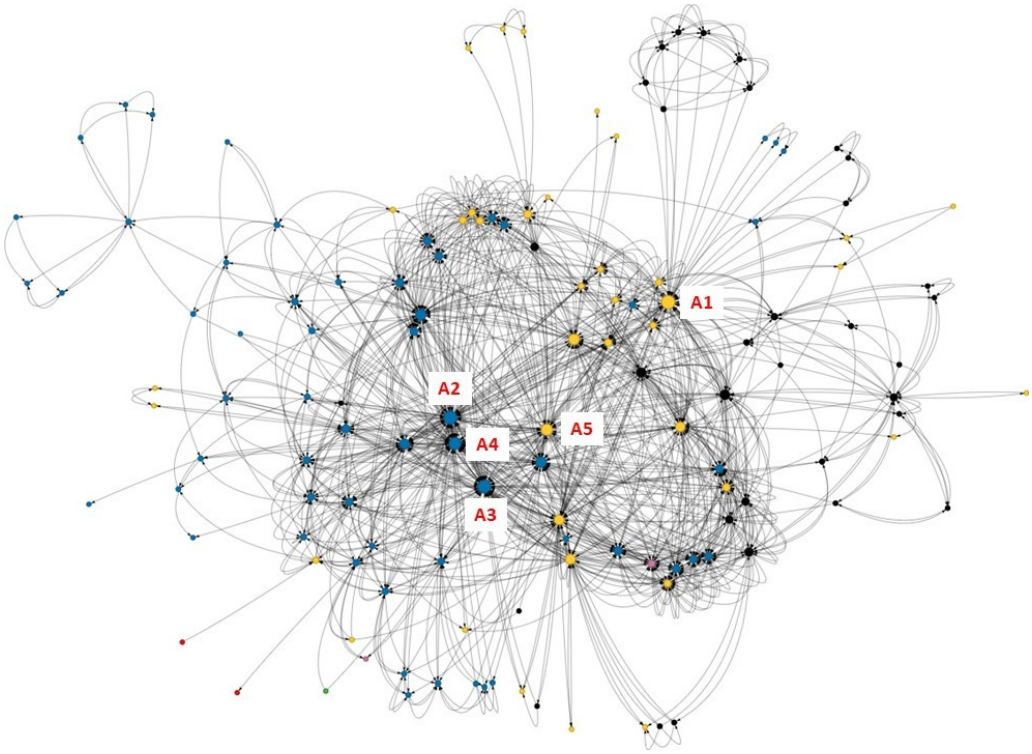

Figure 1. Graphical representation of the pairwise comparisons between the alloys studied in the literature (blue: Ni-based alloys, black: ferritic-martensitic steels, green: BCC HEA, red: FCC HEAs, yellow: austenitic stainless steels (SS), pink: Co-based alloys). The size of nodes is proportional to their centrality degree. Nodes labeled A1 to A5 represent some reference alloys, i.e., those that have been compared the most (see Table 2).

Table 2. Reference alloys from the database in terms of their centrality degree.

Ref.	Alloy	Centrality
(A1)	SS 304	62
(A2)	Inconel 625	58
(A3)	Inconel 600	57
(A4)	Hastelloy N	52
(A5)	SS 316	48

2.3. Gaussian Process for Regression

An important aspect of SR is that it only needs a relative performance index s_{ij} for each pairwise comparison. This means that other information, such as the chemical composition and the microstructure, are not taken into account for the final ranking. The score or rank S_i is subsequently linked to the average chemical content of each alloy i by treating it as a regression problem using a Gaussian process (GP).

A detailed description of GPs can be found elsewhere [25]. A GP is a Bayesian machine learning tool that can perform a flexible regression of an output (the score or rank attributed by SR) as a function of a set of input variables (the alloy's chemical composition) based on a statistical analysis of the data. This method has been used, for instance, to model the yield strength of Ni-based alloys [26], the stability of high entropy alloys (HEAs) [27], or the surface tension of liquid metals [28]. GPs are particularly well adapted to cases where data is scarce and/or scattered [25]. This means that a GP would be the tool of choice in the present case where, as will be explained later, on the one hand, a limited amount of data is available and, on the other, the rank or score inferred by SR may be highly noisy.

2.4. Multi-Objective Optimization Algorithm

The search for alloys that present the best compromise between several predicted properties was made with a modified version of the multi-objective "non-dominated sorting genetic algorithm" NSGA-II [29]. As in most genetic algorithms, the original code works with a population (i.e., a group of alloys), where each one presents a particular genetic code (i.e., chemical composition) with a resulting set of characteristics (i.e., properties). At each generation, the alloys are ranked in a multi-objective perspective through a non-dominated sorting procedure based on a set of targets and constraints. Then, "parents" are selected from the population by using a binary tournament selection based on the rank and crowding distance, from which N "children" are produced by crossing couples of parents and then mutating genes (total population of 2N, typically a few hundred). At the end of an iteration, the Darwinian survival-of-the-fittest standard is applied, where only the N best individuals are kept using the same non-dominated sorting procedure, consequently becoming the parents for the next generation. After several iterations—which takes a few hours depending on the size of the population and the performance of the predictive models used (see later explanation on the use of Thermo-Calc, e.g.)—the genetic algorithm converges to an optimal solution and finds a Pareto set. In other words, it provides a group of alloys where a particular characteristic cannot be further improved without the deterioration of the remaining ones. For example, this approach has been applied to the design of superior Ni-based superalloys [30] and the discovery of strong and light HEAs [31].

3. Results

3.1. Case Study 1: Molten Salt Corrosion

3.1.1. Overall Context: Current State of Corrosion Resistance Data in the Scientific Literature

Molten salt reactors (MSRs) are a type of Generation IV nuclear fission reactor in which the primary coolant is a molten salt mixture [32]. Their design presents several operational and safety advantages over their solid fuel counterparts, such as the continuous removal of Xe after shutdown and more compact components of the primary loop, among others [33]. Moreover, MSRs are also promising in terms of recycling nuclear fuel and improving safety while maintaining an economic edge [34]. Nonetheless, the extreme conditions to which the structural materials are being subjected make it imperative to manufacture alloys with outstanding characteristics, such as a stable microstructure, high-temperature strength, and irradiation resistance, although the most limiting factor probably is their resistance to corrosion in molten salts [35]. The latter might be, for instance, fluorides or chlorides [36]. Unfortunately, corrosion experiments in molten salts are extremely sensitive to testing conditions. It has been shown that the alloy's performance is dependent on the experimental setup, such as the exposure time [37], the salt's composition [38,39], the cover gas [40,41], the relative velocity between the sample and the molten salt [42,43], the crucible [44,45], the temperature [46,47], the alloy's microstructure [48–53], and small variations in the alloy's chemical composition [54–56]. Moreover, it must be taken into account that some of these are difficult to measure, such as the purity of the salt [57] and the real-time evolution of its chemical composition [58].

There have been different data-centric strategies that tackle the modeling of corrosion-resistant alloys, though not particularly under molten salts. For example, Ozdemir et al. [59] used a random forest algorithm to screen the whole compositional space of the HfNbTaTiZr high entropy alloy system and identified a particular composition that presented improved properties for biomedical applications. Their approach for predicting the corrosion potential was validated through subsequent experimental examination. Likewise, Roy et al. [60] also developed an ML model coupled with a descriptors optimization for the prediction of the corrosion rate of multi-principal element alloys in aqueous solutions. They observed that, even though their approach narrowed down the compositional space of potential alloys, they needed a larger dataset and data of better quality in order to improve their predictions of the corrosion rate. On the other hand, Sasidhar et al. [61] recognized that

predicting pitting potential from numerical values exclusively—such as alloy composition, pH, test temperature, and ion concentration—was a rather simplistic approach. So they developed a model that had three distinct components: numerical (developed in [62]), categorial (which took into account the microstructure and type of material), and textual (which included, among others, the description of the test method and heat treatment that were interpreted via natural language processing). Their model helped them understand the contributions of different atomic species in different metallic systems toward pitting resistance. Nevertheless, all such approaches [59–62] were limited to rather conventional data, i.e., where a single property was consistently measured, for limited alloy categories and/or where testing parameters had to be included as inputs, irrespective of whether data was collected manually or automatized using language processing [61]. This makes such methods rather restrictive compared to the present one, which can potentially embrace a very wide set of alloys and conditions provided that comparative pairs of data are available, independently of experimental conditions.

In the following sections of the paper, it will be showed how, by leveraging sparce and diverse data from scientific literature, the proposed method can identify the chemical elements that contribute the most to molten salt corrosion. In addition, it does not require explicitly enviromental factors as inputs (e.g., salt purity, temperature, exposition time, etc.), which in turn reduces the amount of variables necessary for the ML model. Lastly, the objective of the present method is not to accurately predict the mass loss or corrosion rate of a given alloy tested with a given experimental setup, but rather to be able to correctly identify the alloying elements that contribute the most to the materials' performance.

Nonetheless, few attempts have been made toward the design of alloys specifically resistant to molten salt corrosion. For instance, Wang et al. [63] coupled automated characterization with machine learning in order to study the corrosion mechanisms of Cr-Fe-Mn-Ni single-phase face-centered cubic (FCC) HEAs during four days in a LiCl-KCl eutectic salt (44 wt% LiCl—56 wt% KCl) with an addition of 2 wt% $EuCl_3$. They found that those with the highest Ni content were the most resistant, suggesting a sacrificial mechanism where Mn dissolved to avoid Fe from being depleted. On the other hand, Raiman and Lee [64] compiled experimental data—in fluorides and chlorides—from several publications from the period between 1960 and 2016. Their correlation analysis yielded that salt purification played a significant factor in the corrosion rate, followed by experiment setup and salt type.

There a few publications in the scientific literature where selected groups of alloys have been tested in identical experimental conditions, which were later considered for the present study. Since a standardized procedure for corrosion experiments under molten salts does not exist, the data points in the database are highly scattered. A total of 130 different publications have been taken into account, representing a total of 135 different alloys: 38 austenitic stainless steels, 33 ferritic-martensitic steels, 3 HEAs, 2 Co-based, and 59 Ni-based alloys. Some of the experiments were performed in fluorides [65–67], nitrates [68–71], chlorides [72–80], carbonates [81–83], sulfates [84–86], and even mixtures of several of them [87–89]. Some researchers performed their experiments by controlling the purity of the salt [90–92] or choosing a particular cover gas such as Ar [93–95], air [96–98], CO_2 [99], or N [100–102]. The experiments reported in the scientific literature were performed at various temperatures, ranging from 250°C [103–105] up to around 900°C [106–108], whereas some were tested in a non-isothermal fashion [109–111]. The times of exposure were also very diverse, where some alloys were studied for a few hours [112–114] up to several weeks [115–117]. Even the chosen crucibles were distinct, being as different as oxides [118–121], glassy carbon [122–124], graphite [125–127], or stainless steels [128–130], among others. The assessment of corrosion also involved various methods, like measuring a weight change [131–133], the thickness of a corroded layer [134–136], or the corrosion current during an electrochemically monitored experiment [137–139].

3.1.2. Application of the Method: From SpringRank to Machine Learning Prediction of Corrosion Resistance

As corrosion is an electrochemical phenomenon that can take place via different attack modes—with each one having its own mechanisms [140]—the choice of a metric that faithfully reflects the alloy's resistance is not an obvious one. For the following, two criteria were used to express the metal's performance against molten salt corrosion:

- The absolute value of the mass change (both gain and loss) after a given exposure time to reflect the fact that a good alloy would either dissolve slowly [141], grow gradually a stable oxide scale [81], or even passivate [142]. On the contrary, an important weight loss [143] would indicate a fast dissolution and poor behavior, whereas a large gain in mass would suggest a rapid oxide growth [69], associated with a high risk of scale spallation [107] and eventually to an accelerated metal loss. The possibility of an important weight gain balanced by a subsequent weight loss is not considered in this approach.
- The corrosion rate measured by electrochemistry (a corrosion current density [144]) or attack depth [136].

Consequently, the comparative index s_{ij} was given by the absolute value of the ratio between the alloy i that had the highest mass change (or corrosion rate) divided by that of its competitor j. A total of 4306 pairwise comparisons were used as inputs for the ranking.

Figure 1 shows the network generated from all the pairwise comparisons. Each node is an alloy, and the edges correspond to pairs of alloys that have been compared in the scientific literature. From its general structure, it can be seen that it is a sparse graph since not all nodes are connected to all others; in fact, some of them are just compared against only one alloy. This comes from the usual practice where an experimental study focuses on examining a particular commercial alloy against homemade ones in order to analyze the impact of minor changes in their chemical composition, as in the case of N1, N2, and Inconel 713LC [56]. A clear setback from the presented strategy is that all the considered alloys (i.e., nodes) must be connected: the resulting graph has to be a closed network without the presence of isolated islands, as shown in Figure 1. Nevertheless, some HEAs [145–147], Ni-based [148–153], Fe-based [154–157], and other [158–160] interesting alloys were found in the scientific literature, but unfortunately, they were not included in the current study simply because they were not also compared to other alloys present in the database in identical experimental conditions.

It is possible to study the structure of the network (Figure 1) in terms of graph theory. Even though there are several ways to identify the most important nodes inside a network [161], the centrality degree provides some insight, if assumed that the network is undirected as a first approximation. This parameter is defined as the total number of nodes (alloys) connected to a particular one. In other words, it serves as an idea of which alloys were used as major references for molten salt corrosion tests (Table 2) and the number of alloys against which they had already been compared in the scientific literature.

Figure 2 shows the overall ranking determined by SR. The lower the score, the more performant the alloy. (The best one is at the bottom of the chart). It is possible to see that alloys with a face-centered cubic (FCC) structure (SS and Ni-based alloys) are almost always ranked better than ferritic-martensitic (FM) steels and an HEA with a body-centered cubic (BCC) structure: the top 20% alloys have an FCC structure.

Table 3 shows the best ten alloys according to SR. (The complete list is presented in Appendix A). Even though almost all of them have a high content of NI, with the notable exception of an FCC HEA, it is possible to identify different clusters according to their chemical composition. The first group corresponds to Ni-rich alloys with a very high content in Mo (15–18 wt.%), with also Cr (6–23 wt.%) (MoNiCr [16], VDM 59 [88,162], Hastelloy C4 [162,163], and Hastelloy N [16,17,65,82,90,108,123,126,127,137,164–172]. The second one corresponds to Ni-rich alloys with a high content in Al (~5–6 wt.%), Si and Nb with a smaller amount of Cr and no Mo (N101 [39,173], N1 [56], N102 [39,173], and N2 [56]). Other alloys are the FCC HEA $Al_{0.1}CoCrFeNi$ [174] and Kubota UCX [133], which

might be considered as a third group in that they have in common a high Cr content (like VDM 59, which is also rich in Mo). According to the literature, Mo would slow down dissolution [18,175] and/or favor passivation [76], whereas Al would promote the slow growth of a stable and protective layer of alumina (Al_2O_3) [55,176]. Cr would induce the formation of a defensive oxide scale as well (chromia—Cr_2O_3), which seems somewhat efficient in fluorides [177] but not in chlorides [74,178]. It is noticeable that even though SR was not fed with any information regarding chemical composition, it seems able to identify and deduce indirectly which elements should contribute the most to the alloy's molten salt corrosion performance starting from macroscopic measurements (i.e., the mass change or corrosion rate).

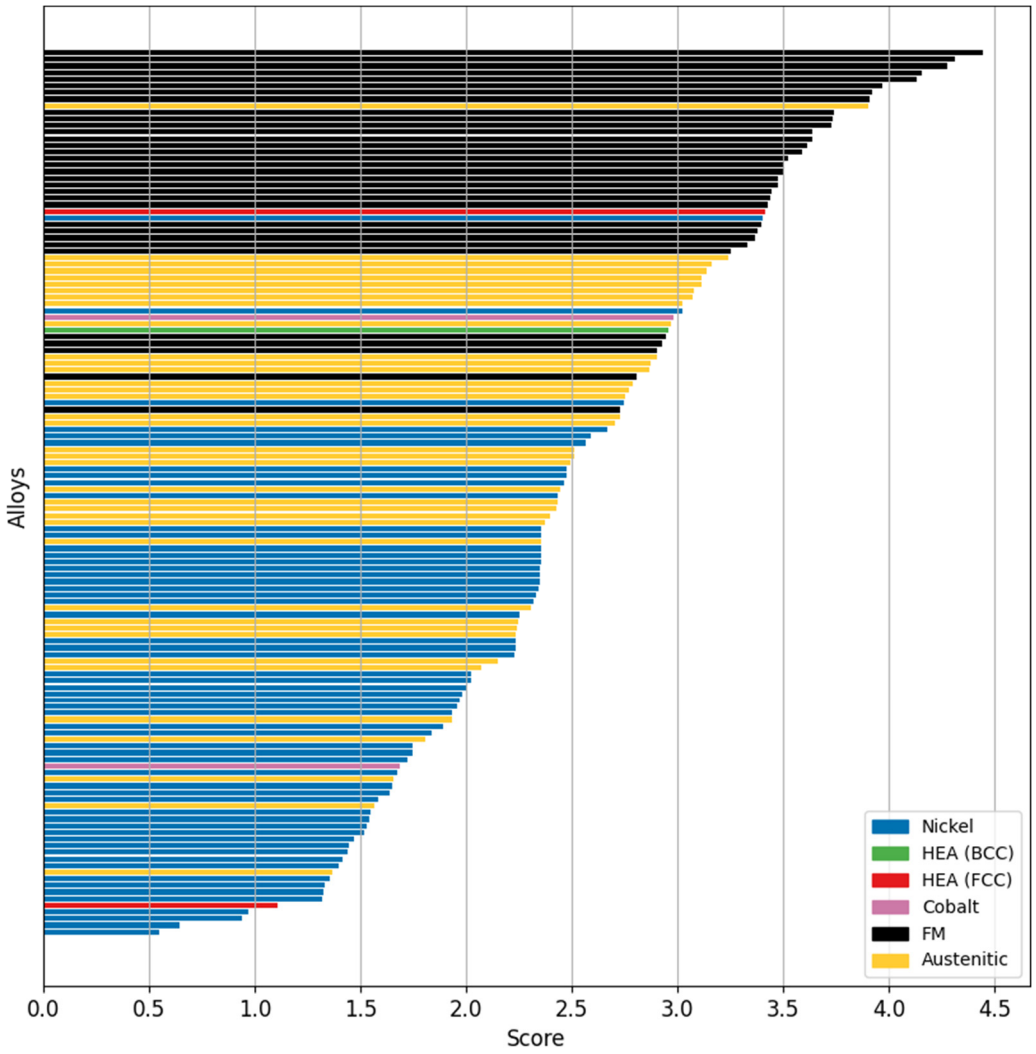

Figure 2. Overall alloy rank analyzed in molten salt corrosion experiments. (The complete list of alloys with their chemical composition and individual score S_i can be found in Appendix A of this manuscript). "Austenitic" stands for "austenitic stainless steels".

The next step was to learn the score inferred by SR as a function of alloy composition using GP regression. In Table 4, the spectrum of the possible values for each chemical species is displayed, characterized by its considerable breadth. The maxima indicate that all alloys relying on a principal element are based on either Fe, Ni, or Co.

Table 3. SR's prediction of the top-ten alloys with their average chemical composition (in wt.%).

Alloy	Cr	Ni	Fe	Mo	Al	C	Cu	Si	Mn	W	Co	Ti	Nb	V	S_i
MoNiCr	6.77	74.81	0.7	17.41	0.005	0.001	0.01	0.162	0.059	0.0075	0.036	0.001	0.011	0.022	0
N101	12	76.92	0.11	-	5.8	0.06	-	2.04	-	-	0.06	1.05	1.96	-	0.54
N1	12	77.38	0.05	-	6	0.05	-	2.03	-	-	-	0.49	2	-	0.65
N102	12.5	73.95	0.15	-	6.1	0.04	-	4.67	-	-	0.06	0.53	2	-	0.94
N2	11.98	74.6	0.05	-	5.95	0.05	-	4.95	-	-	-	0.49	1.93	-	0.97
$Al_{0.1}$CoCrFeNi	22.84	25.73	24.48	-	1.17	-	-	-	-	-	25.78	-	-	-	1.11
Hastelloy C4	16	65.105	1.5	15.5	-	0.005	-	0.04	0.5	-	1	0.35	-	-	1.32
VDM 59	23	59.795	0.75	15.75	0.25	0.005	-	0.05	0.25	-	0.15	-	-	-	1.32
Kubota UCX	41.1	47.81	5.5	1.43	-	0.48	-	2.16	-	-	-	-	1.52	-	1.33
Hastelloy N	7	73.105	2	16	0.125	0.06	0.175	0.5	0.4	0.25	0.01	0.125	-	0.25	1.35

Table 4. Minimum and maximum values for each chemical element in the database.

Element	Cr	Ni	Fe	Mo	Al	C	Cu	Si	Mn	W	Co	Ti	Nb	V
Min (wt.%)	0.125	0.125	0.05	0.175	0.005	0.001	0.01	0.03	0.005	0.0075	0.01	0.001	0.011	0.022
Max (wt.%)	41.1	79.62	99.345	28.5	10.7	5.17	3.5	5	27	26.1	51.7	3.15	5.125	1.16

Figure 3 shows the comparison between the overall score inferred by SR and the one predicted by the GP, from which several distinct features can be observed. First, there is an associated uncertainty along the horizontal axis, where certain alloys have been attributed a different score by SR, although having somewhat close chemical compositions (e.g., Hastelloy N and MoNiCr from Table 3), implying that the GP model predicts similar values of S_i. Second, there is an uncertainty along the vertical axis, where those scores assigned by SR are very similar to one another but very different from those predicted by GP due to their different chemical composition. Third, there seems to be a cloud of data points around a score of 3.5, which are mostly those alloys with an FM microstructure. Fourth, it is interesting to see that according to SR, most austenitic steels and Ni-based alloys are grouped in scores between 1.5 and 3, although the GP predicts that all alloys up to a score of approximately 2.3 are purely Ni-based alloys, whereas the austenitic steels are mostly grouped between scores of 2.3 and 2.8. Nonetheless, it is possible to see a fair agreement between the scores by SR and GP.

However, the relatively high scatter indicates a potential error in predictions, but the good overall agreement shows that the trends are correctly identified. Due to their Bayesian nature, GPs provide an error estimate along with their predictions, inferred from the data's statistical analysis. This can be exploited to design alloys in a robust manner by taking the predictive error into account. (This will be shown in the second case study.) In any case, when designing alloys with complex characteristics, like corrosion resistance, optimizing by following correct trends would still represent a potential improvement compared to a complete absence of predictive tools. Works are currently ongoing toward this objective of designing alloys for future molten salt nuclear reactors. In the meantime, as exposed in the following section, the approach has also been applied to model the wear resistance of hard-facing alloys, through the analysis of a smaller dataset with a different network structure. The model has then been used to design new alloys by combinatorial optimization, followed by experimental validation, to illustrate the ability of the method to extract correct trends from a reduced and scattered pairwise comparative dataset and to make reliable predictions.

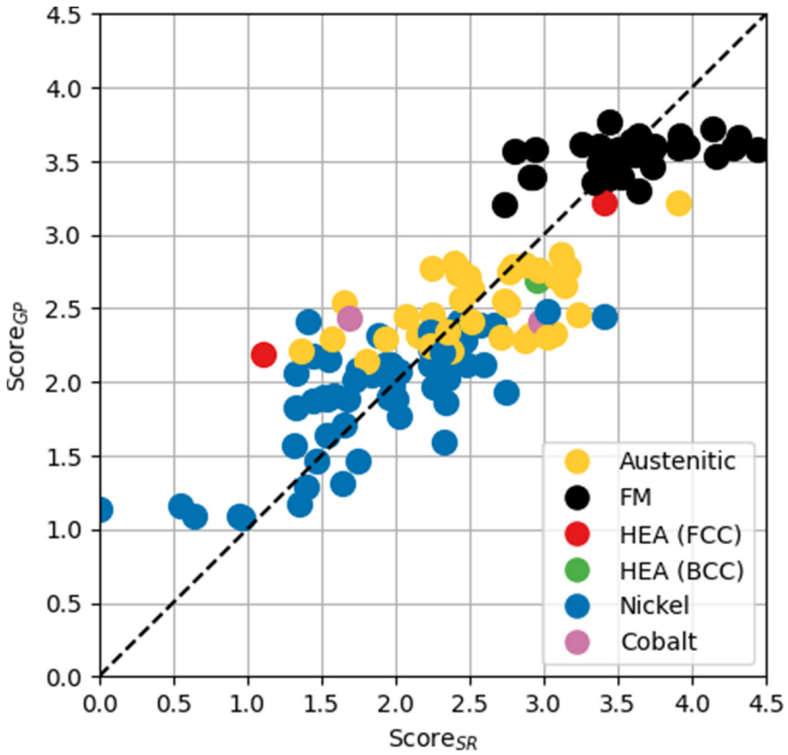

Figure 3. Comparison between the scores computed by SR and GP. "Austenitic" stands for "austenitic stainless steels".

3.2. Case Study 2: Design of Wear-Resistant Hard-Facing Alloys

3.2.1. Current State of Wear-Resistance Data and Application of the Proposed Method

The prevention of wear on structural components can be achieved by depositing coatings of so-called hard-facing alloys. Consequently, the part can globally keep its bulk mechanical properties, including a good combination of strength, ductility, and toughness, while the hard coating faces external contact stresses, avoiding surface abrasion or erosion. Although the wear resistance of pure metals or solid solution alloys has been found to correlate mainly to hardness, this is not the case when a superior wear performance is to be obtained through complex microstructures [179]. In such cases, specific testing must be undertaken. However, the material's response to wear is, like in the corrosion case, highly sensitive to the testing conditions. It has been shown that hard-facing alloy performance is dependent on the experimental conditions, such as differences in the chemical composition [180,181] and microstructure [182] of the alloy, the deposition technique used to produce the coatings [183], the temperature [184], the atmospheric humidity [185], and the experimental setup itself [186]. The latter can involve, for instance, pin-on-disc, ball-on-disc, plate-on-plate, disc-on-disc geometries, etc. The counter material can be identical to the tested one or be a very hard material, e.g., a ceramic or cermet. The relative movement of both parts can be linear or rotary, with variable testing parameters like friction velocity, contact force or pressure, total length of friction, absence or presence of a lubricant, nature of the latter, etc. Thus, the measurement of wear itself is also different across studies. Indeed, a wear rate is usually expressed by the unit length of friction, but it can refer to a loss in mass or thickness, to the depth or the volume of the wear track, etc. Therefore, the problem is of the same nature as for molten salt corrosion: it is almost impossible to gather a significant dataset of materials tested in identical conditions. However, in several literature sources [180–184,187–192], two or more alloys have been characterized in the same manner, rendering possible a pairwise comparison strategy, provided that some alloys are present in different sources, to allow a proximity ranking. The so-obtained dataset is constituted of 15 Fe-based alloys, 14 Ni-based alloys, and 6 Co-based

alloys. The resulting network is presented in Figure 4 in a similar way as in the previous section. Several comments can be made: (i) with only 35 alloys, the size of the dataset remains rather small; (ii) there is also a limited number of edges; (iii) Stellite 6 is by far the most central alloy, i.e., the one most often used as a reference in the experimental studies, which seems normal since it is probably the most popular hard-facing alloy, followed by Norem 02, which is one of the most studied material as a potential Co-free replacement for Stellite alloys in the nuclear industry (this will be explained later); and (iv) besides such reference alloys, many materials have only been compared a few times. It is therefore interesting to see on the one hand if such a network structure can be exploited by a pairwise comparison algorithm and, on the other, if compositional trends can be learned by a GP to build a statistical regression model, which may eventually be used to design new highly performant alloys by combinatorial optimization.

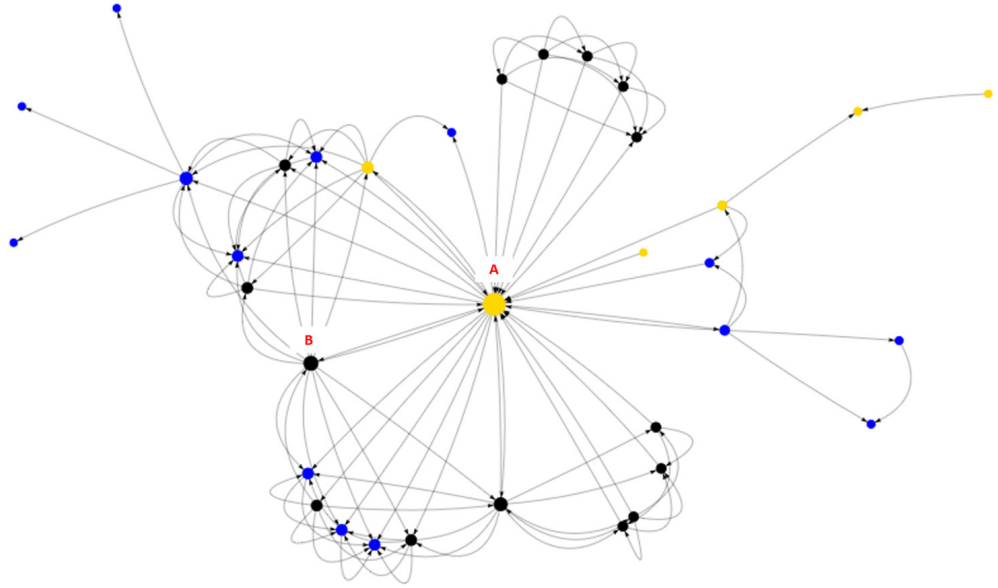

Figure 4. Graphical representation of the pairwise comparisons between the alloys studied in the literature (blue: Ni-based alloys; black: Fe-based alloys; yellow: Co-based alloys). The size of nodes is proportional to their centrality degree. Nodes labeled A and B correspond to Stellite 6 and Norem 02, respectively.

The method associating the pairwise comparison algorithm and a GP to produce a predictive model of alloy performance as a function of composition is similar to the one of the first case study. To illustrate a different possibility, the wear resistance rank is here fitted by the GP instead of the score S_i. The rank predicted by GP is plotted in Figure 5 against the one determined by SR.

Despite the small number of data points and a substantial dispersion, a fair agreement is obtained, indicating that the model seems capable to capture compositional trends governing the wear resistance of alloys. The originality here is to incorporate this model into an alloy design scheme by combinatorial multi-objective optimization, which is described hereafter.

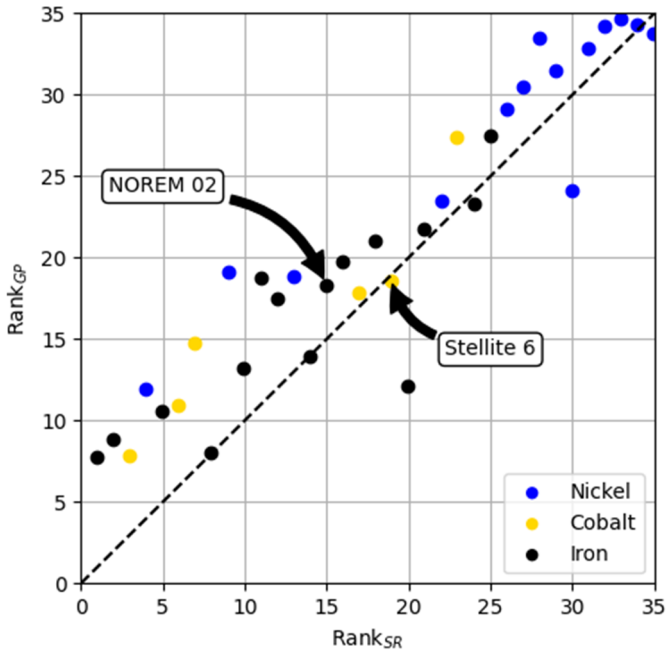

Figure 5. Rank predicted by the GP regression model as a function of the rank attributed by the pairwise comparison algorithm (SR, see Appendix B) for the alloys of the database (being either Fe-based, Cot-based, or Ni-based). Stellite 6 and Norem 02 alloys are highlighted.

3.2.2. Design of Superior Alloys: Objectives and Constraints in the Optimization Algorithm

Hard-facing alloys are, among others, used in the primary circuit of nuclear power plants, as wear-resistant coatings on parts of valves and pumps, as well as on rod control mechanisms. The most used material is Stellite 6, a Co-based alloy rich in Cr, hardened by carbides. It presents a very good combination of corrosion resistance, wear resistance, and ability to be deposited by welding-type processes. However, it suffers from a major drawback: following wear during service, alloy particles are driven in the primary circuit, and their Co is activated in the long-period ^{60}Co radioactive isotope, which is at the origin of a significant part of the radiation dose received by maintenance workers in nuclear power plants and complicates future dismantling. Vast research has been made toward the development of Co-free alloys, like Norem 02 [23] or Nitromaxx [23], with mixed results, so the search for a better alternative is still ongoing. An approach is presented here to design new Fe-based, Co-free hard-facing alloys via a multi-objective combinatorial optimization. The latter was performed by a genetic algorithm [30], aiming among others at:

- Maximizing the wear resistance predicted by the new model described above, associating a pairwise comparison algorithm and GP regression; this corresponds to minimizing the predicted rank. Nevertheless, to improve the robustness of the design process, minimization was not performed on the mean predicted rank but on the mean plus a standard deviation. Indeed, being statistical tools, GPs calculate the predictive distribution of the model output so that its standard deviation can be seen as a predictive error estimate. Doing so, a pessimistic rank is obtained, which should better guarantee that the designed alloys will actually match the objective.
- Targeting a specific type of as-solidified microstructure since alloys will be deposited by welding-type processes. It must be made of a metallic solid solution matrix reinforced by hard phases such as carbides and/or borides, as in most existing hard-facing alloys.
- Maximizing the chromium content in the solid solution matrix ("free Cr") to ensure corrosion resistance.

Microstructural features were predicted by computational thermodynamics, using the "calculation of phase diagrams" (Calphad) software Thermo-Calc (version 2018, Stockholm, Sweden) along with the TCFE9 database for Fe-based alloys. The Scheil model was employed, which is adapted to the simulation of as-solidified microstructures.

The genetic algorithm was configured to explore the compositional space of Table 5.

Table 5. Compositional space explored in alloy design (in wt.%). Iron is the balance element.

Element	Cr	Mn	Mo	V	W	Ni	Nb	Si	C	B	N
Min	15	0	0	0	0	0	0	0	0	0	0
Max	40	5	3	3	10	5	3	3	5	2	1
Step	0.1	0.1	0.1	0.1	0.1	0.1	0.1	0.1	0.01	0.01	0.01

After different optimization runs, the algorithm produced hundreds of Pareto-optimal alloys, presenting different trade-offs between, among others, predicted wear resistance (rank) and corrosion resistance (free Cr). Among all designed materials, four alloys were selected (hereafter named AS1, AS2, AS3, and AS4), exhibiting different compromises between such characteristics. Their composition is given in Table 6.

Table 6. Composition of selected alloys (in wt.%). Iron is the balance element. Only a compositional range is given for AS4 due to confidentiality issues.

Alloy	Cr	Mn	Mo	W	Ni	Nb	Si	C	B
AS1	25	2	0.2	0	1	1.1	0	1.2	1
AS2	22	0	0.2	0	0.3	1.1	0.6	1.2	1
AS3	21	2.2	0	0	6.7	2	0	0.45	0.7
AS4	15–25	<3	<5	<3	5–10	<3	<3	<1.5	<1.5

3.2.3. Experimental Validation of the Designed Alloys with Their Corresponding Rank

Selected alloys, along with two reference alloys (Norem 02 and the best alloy in terms of wear resistance identified by SR from the database [23,181], hereafter called "FeCrB"), were produced (300g ingots) by induction melting in a cold crucible. In agreement with the industrial process foreseen for this kind of materials, alloys were studied in the as-solidified state, with a microstructure similar to one of welded deposits. Specimens were investigated by a set of microstructural characterization techniques, such as X-ray diffraction, transmission electron microscopy (TEM), scanning electron microscopy (SEM) with energy dispersive spectroscopy (EDS), and electron backscatter diffraction (EBSD). W ear testing was undertaken at room temperature without lubricant using a rotary tribometer with a ball-on-disc geometry, with a 6 mm diameter tungsten carbide ball and a disc of the tested material polished with silicon carbide abrasive paper down to grade P1200. The contact force was 8 N, and the relative ball-track velocity was 1.5 mm.s^{-1}, for a total track length of 150 m, with a wear track diameter of 16 mm. The worn volume was then calculated as the product between the circumference and the cross-section area of the wear track, determined by profilometry after observing the track from above with an optical confocal microscope. (The cross-section area was averaged from eight locations around the track.) The worn volume was then divided by the contact force and the total track length to obtain the specific wear rate. In addition to in-house-produced alloys (AS1, AS2, AS3, AS4, Norem 02, and FeCrB), a disc of commercially available Stellite 6 was tested in identical conditions for comparison purposes. An in-depth analysis of the found microstructures and their general properties can be found elsewhere [23].

Wear resistance results are displayed in Figure 6, plotted as the measured specific wear rate versus the wear rank resistance predicted by the model.

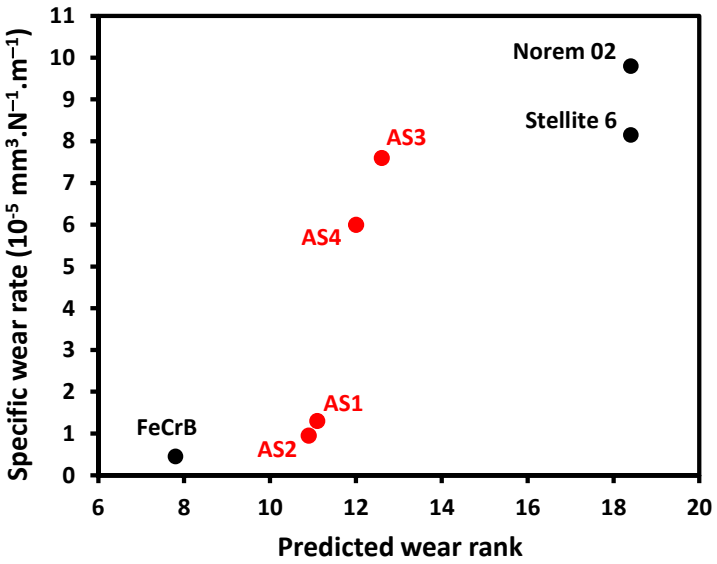

Figure 6. Measured specific wear rate as a function of the robust wear rank predicted by the model for reference alloys (Norem 02, Stellite 6, and FeCrB) and the newly designed alloys (AS1, AS2, AS3, and AS4).

Although there is no simple relation between both quantities, the predicted trend is satisfactory since the experimental measurements are in the same order as the predicted wear rank. This demonstrates the applicability of the new modeling method associating a pairwise comparison algorithm with a regression model. The best alloys are the already reported alloy FeCrB and our new alloys AS1 and AS2, with measured wear rates well below those of industrial alloys Stellite 6 and Norem 02. Alloy FeCrB performs slightly better than alloys AS1 and AS2, but its predicted free Cr concentration (12.8 wt.%) is lower than that of alloys AS1 (17.2 wt.%) and AS2 (15.9 wt.%), with an associated risk of lower corrosion resistance. All three alloys (FeCrB, AS1, and AS2) are rather brittle, with an experimental strain to failure around 3–4% in compression, rendering their application somewhat risky. Conversely, all other alloys could be strained to at least 10% in compression and appear more ductile, associated with a potentially safer use. Norem 02 is less resistant to wear, but among the Fe-based alloys, it is the one with the highest free Cr concentration: 19.4 wt.% vs. 17.7 wt.% for AS3 and 15.3 wt.% for AS4. (Not being Fe-based, Stellite 6 cannot be directly compared on this criterion.) Both alloys AS3 and AS4 could therefore be considered as interesting trade-offs compared to Norem 02, with a slightly reduced corrosion resistance but a substantial gain in wear resistance between ~20% and ~40%. Results are summarized in Figure 7 in terms of compromise between wear resistance and potential corrosion resistance of Fe-based alloys.

Aiming for a low wear rate and a high free Cr concentration, all alloys shown in Figure 7 would be Pareto-optimal except for AS4. Nevertheless, considering separately brittle and ductile alloys makes all of them Pareto-optimal within their own category.

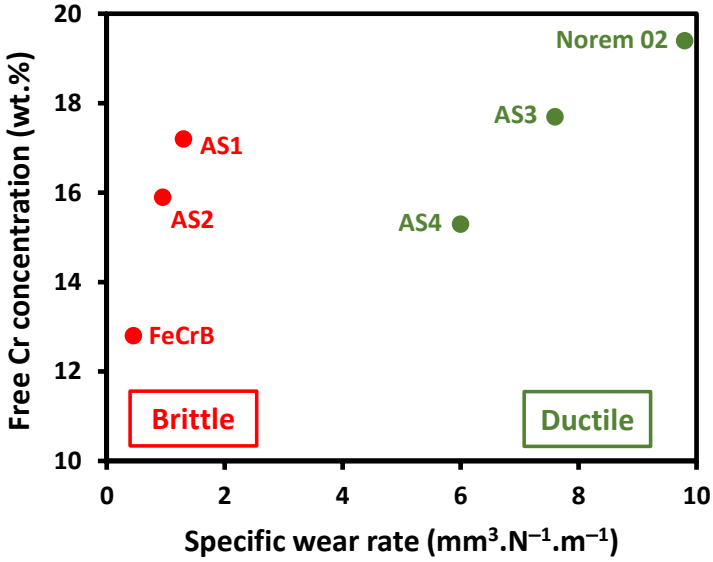

Figure 7. Dependency of the specific wear rate with respect to the free Cr concentration (wt.%).

4. Conclusions and Perspectives

In the present paper, a method is developed to exploit data on complex material behaviors that are impossible to analyze with standard machine learning techniques. In this respect, it cannot be compared to others and stands as a unique tool to tackle data in which the comparative structure is the only exploitable feature. This method is here applied to particular case studies: the corrosion of structural materials in molten salts and the wear resistance of hard-facing alloys. A pairwise comparison algorithm—SR—is used to evaluate the properties of pairs of alloys tested in identical conditions in a given study. By also considering some common alloys but tested with different experimental setups by different teams, an overall ranking between materials is deduced. At this first stage, no information or data is needed on important characteristics, such as alloy composition, processing, or microstructure: ranking is made on material performance only. As such, SR is able to infer implicitly which elements contribute the most to the materials performance in each case study. The obtained score—or rank—is then fitted as a function of alloy composition by a GPs regression, as the data points are scarce and noisy.

For the first case—the resistance to corrosion by molten salts—a database is built from alloys reported in the scientific literature. The dataset constitutes a rather dense network of 135 materials tested in 130 separate investigations (where at least two alloys are compared in identical conditions), resulting in more than 4000 pairwise comparisons from which SR is able to identify which constituents (e.g., Mo, Al, Cr, etc.) contribute the most to corrosion resistance. Then, the score inferred by SR is fitted by a GP regression as a function of 14 compositional variables. There is a fair agreement between the actual and predicted scores, and the model is able to reproduce some compositional trends that are expected from a qualitative physical analysis (e.g., the role of the base element Fe or Ni and their alloying constituents). Nonetheless, it is hoped that relevant interactions are also captured and that a quantitative exploitation of such a model is possible.

This final point is demonstrated in the second case study, the wear resistance of hard-facing alloys. The pairwise network is much smaller than in the previous case study (35 materials tested in 11 separate investigations for a total of 106 pairwise comparisons) and presents a smaller number of ramifications. However, it is shown that the obtained model can be exploited to make reliable predictions and, as such, be used to design new performant alloys by combinatorial optimization, which is here performed via a multi-objective genetic algorithm. At this stage, in addition to the machine learning model built using SR and GP, the microstructure resulting from both composition and processing is taken into account through thermodynamics using the Calphad software Thermo-Calc, e.g.,

to aim for a certain type of solidification path and structure. Four new alloys have been selected, elaborated, and compared in identical testing conditions to concurrent materials. Some of the designed alloys display interesting trade-offs between several characteristics. In any case, the better the predicted wear resistance rank, the lower the actual wear rate, indicating that the new model is able to fit existing data and predict correct trends. This notion of trends is fundamental in alloy design and central to the present approach. Indeed, obtained models being based on comparative data that are, by nature, only comparable within a given study but incomparable across different studies, their interpretability can only be comparative itself. The inferred rank or score does not have any absolute physical meaning, but compositional trends are correct. At best, when a prediction is made for a new alloy, the user may try to find, among known alloys in the database, those that possess similar ranks or scores. Looking at the published works where the associated data came from, it could be possible to estimate the potential performance of the new alloy if it were to be tested in those particular conditions.

As a final point, it would be interesting to develop a more homogeneous database—e.g., having every single pairwise comparison tested in identical conditions—and to incorporate alloys in the analysis that present unique chemical compositions and microstructures (e.g., HEAs, intermetallics, and duplex steels, just to name a few). In fact, even if the method proved to be able to tackle successfully incomplete datasets on complex characteristics and although trends are exploitable, the level of scatter—hence uncertainty—remains substantial. This, in the end, also calls for more standardized testing protocols and cross-validation procedures between institutions [193–195]. Nonetheless, the method proposed in this paper should be capable to analyze other complex materials characteristics, i.e., irradiation resistance, formability, hydrogen embrittlement, etc., and to accelerate the search and design of alloys with superior properties.

Author Contributions: Conceptualization, R.H., L.R. and F.T.; methodology, R.H., L.R., A.F., G.R. and F.T.; software, G.R. and F.T.; validation, R.H. and L.R.; formal analysis, R.H. and L.R.; investigation, R.H. and L.R.; resources, J.D., A.F., G.R. and F.T.; data curation, R.H., L.R. and L.M.; writing—original draft preparation, R.H. and F.T.; writing—review and editing, L.M., F.B.-C., A.F. and G.R.; visualization, R.H. and L.R; supervision, A.F. and F.T.; project administration, J.D., A.F. and F.T.; funding acquisition, F.B.-C. and J.D. All authors have read and agreed to the published version of the manuscript.

Funding: The work of L. Rateau (2019–2023) on wear-resistant alloys has notably benefited from the cofunding of Framatome Company and the Association Nationale de la Recherche et de la Technologie (ANRT), under agreement CIFRE-2019/1194. The work on molten salt corrosion (notably that of R. Herschberg in 2023–2024) has benefited from French government grants managed by the Agence Nationale de la Recherche (ANR) under the France 2030 program DIADEM; references ANR-22-PEXD-0003 and ANR-22-PEXD-0005.

Data Availability Statement: The original contributions presented in this study are included in the article. Further inquiries can be directed to the corresponding author.

Acknowledgments: Authors thank the technical contribution of the staff of Centre Technique Framatome—Le Creusot to the measurement of wear resistance. The technical staff of MINES (M. Haering and C. Varillon) is acknowledged for the elaboration of model alloys.

Conflicts of Interest: Authors Lisa Rateau, Jean Dhers were employed by the company Framatome. The remaining authors declare that the research was conducted in the absence of any commercial or financial relationships that could be construed as a potential conflict of interest.

Appendix A. Ranking of the Alloys Tested Under Molten Salts Experiments

Alloy	Cr	Ni	Fe	Mo	Al	C	Cu	Si	Mn	W	Co	Ti	Nb	V	S_i
MoNiCr	6.77	74.81	0.7	17.41	0.005	0.001	0.01	0.162	0.059	0.0075	0.036	0.001	0.011	0.022	0
N101	12	76.92	0.11	-	5.8	0.06	-	2.04	-	-	0.06	1.05	1.96	-	0.54
N1	12	77.38	0.05	-	6	0.05	-	2.03	-	-	-	0.49	2	-	0.65
N102	12.5	73.95	0.15	-	6.1	0.04	-	4.67	-	-	0.06	0.53	2	-	0.94
N2	11.98	74.6	0.05	-	5.95	0.05	-	4.95	-	-	-	0.49	1.93	-	0.97
$Al_{0.1}$CoCrFeNi	22.84	25.73	24.48	-	1.17	-	-	-	-	-	25.78	-	-	-	1.11
Hastelloy C4	16	65.105	1.5	15.5	-	0.005	-	0.04	0.5	-	1	0.35	-	-	1.32
VDM 59	23	59.795	0.75	15.75	0.25	0.005	-	0.05	0.25	-	0.15	-	-	-	1.32
Kubota UCX	41.1	47.81	5.5	1.43	-	0.48	-	2.16	-	-	-	-	1.52	-	1.33
Hastelloy N	7	73.105	2	16	0.125	0.06	0.175	0.5	0.4	0.25	0.01	0.125	-	0.25	1.35
SS 310HCbN	25	20.5	52.28	-	-	0.07	-	0.75	1	-	-	-	0.4	-	1.37
GH 3535	6.94	70.95	3.93	16.6	0.18	0.53	-	0.32	0.5	0.05	-	-	-	-	1.4
Incoloy 800HT	21	32.5	45.395	-	0.5125	0.08	-	-	-	-	-	0.5125	-	-	1.41
Incoloy 825 (3)	22.69	42.574	26.84	3.28	-	-	2.79	-	0.486	-	-	1.34	-	-	1.44
Hastelloy C2000	23	57.355	1.5	16	0.25	0.005	1.6	0.04	0.25	-	-	-	-	-	1.45
N103	20	66.355	0.05	-	6	0.05	-	5	0.005	-	0.04	0.5	2	-	1.47
Ni-26W-6Cr	5.86	66.123	0.54	1	-	0.037	-	0.14	-	26.1	-	0.2	-	-	1.52
Hastelloy C22	22	57.28	3	13	-	0.005	-	0.04	0.25	3	1.25	-	-	0.175	1.53
KhN62M	23.2	63.02	0.47	13	0.11	-	0.01	0.03	0.03	0.05	-	0.08	-	-	1.54
Haynes 263	20	51.49	0.35	6	0.3	0.06	-	0.2	0.4	-	20	1.2	-	-	1.55
SS S35140	21	26	48.575	1.5	-	0.05	-	0.375	2	-	-	-	0.5	-	1.57
Haynes 75	20	73.525	5	-	-	0.075	-	0.5	0.5	-	-	0.4	-	-	1.58
Inconel 713LC	12	79.45	-	-	5.9	0.05	-	-	-	-	-	0.6	2	-	1.64
Haynes 214	16	76.1	3	-	4.5	0.05	-	0.1	0.25	-	-	-	-	-	1.65

Alloy	Cr	Ni	Fe	Mo	Al	C	Cu	Si	Mn	W	Co	Ti	Nb	V	S_i
SS 309	23	14	59.8	-	-	0.2	-	1	2	-	-	-	-	-	1.66
Inconel MA754	20	78.15	1	-	0.3	0.05	-	-	-	-	-	0.5	-	-	1.68
Haynes 25	20	10	1.5	0.5	-	0.1	-	0.2	1.5	15	51.2	-	-	-	1.68
Hastelloy G	22.25	45.1	19.5	6.5	-	0.025	0.75	0.5	1.5	0.5	1.25	-	2.125	-	1.72
Kubota KHR45	36.2	39.98	19.1	1.5	-	0.4	-	1.31	-	-	-	-	1.51	-	1.75
N3	20.05	66.34	0.05	-	6.05	0.05	-	4.98	-	-	-	0.5	1.98	-	1.75
Multimet	21.25	20	30.38	3	-	0.12	-	0.5	1.5	2.5	19.75	-	1	-	1.80
Haynes 244	8	61.835	1	22.5	0.25	0.015	-	-	0.4	6	-	-	-	-	1.84
Haynes HR224	20	48.7	27.5	-	3.8	-	-	-	-	-	-	-	-	-	1.89
SS 310S	25	20.5	52.71	-	-	0.04	-	0.75	1	-	-	-	-	-	1.93
Inconel 718	19	53.385	17	3.05	0.5	0.04	0.15	0.175	0.175	-	0.5	0.9	5.125	-	1.93
Hastelloy G35	33	57.225	1	8	0.2	0.025	-	0.3	0.25	-	-	-	-	-	1.96
Rene 41	19	52.39	2.5	9.75	1.6	0.06	0.25	0.25	0.05	-	11	3.15	-	-	1.97
Haynes 282	20	56.865	0.75	8.5	1.5	0.06	-	0.075	0.15	-	10	2.1	-	-	1.98
Hastelloy C	16	73.16	5.5	-	-	0.04	-	0.05	0.5	4.75	-	-	-	-	2.00
Inconel 601	23	61.35	13	-	1.35	0.05	0.5	0.25	0.5	-	-	-	-	-	2.02
Inconel 702	15.5	79.62	1	0	3.25	-	-	-	-	-	-	-	-	-	-
Kaeri Super alloy 4	8	36	55.485	-	-	-	-	0.25	0.25	-	-	-	-	-	2.07
ATI 332Mo	21.5	33	41.025	2.5	-	0.05	-	0.25	1.25	-	-	-	0.425	-	2.15
Kubota KHR35	22.8	35.96	36.6	1.47	-	0.39	-	1.31	-	-	-	-	1.47	-	2.23
RA 333	25.5	45.5	17.085	3.25	-	0.04	-	1.125	1	3.25	3.25	-	-	-	2.23
Incoloy 825	21.5	42	29.475	3	0.1	0.025	2.25	0.25	0.5	-	-	0.9	-	-	2.23
Sanicro 25	22.5	25	43.15	-	-	0.05	3	0.2	0.5	3.6	1.5	-	0.5	-	2.24
RA 330	19	35.5	42.71	-	-	0.04	0.5	1.25	1	-	-	-	-	-	2.24
SS 304H	19	9.5	70.055	-	-	0.07	-	0.375	1	-	-	-	-	-	2.25

Alloy	Cr	Ni	Fe	Mo	Al	C	Cu	Si	Mn	W	Co	Ti	Nb	V	S_i
Hastelloy C276	15.5	57.28	5.5	16	-	0.005	-	0.04	0.5	3.75	1.25	-	-	0.175	2.25
06KhN28MDT	23.5	27	42.22	2.75	-	0.03	3	0.4	0.4	-	-	0.7	-	-	2.31
Incoloy 20	20	33.75	37.22	3.5	-	0.03	3.5	0.5	1	-	-	-	0.5	-	2.32
Hastelloy S	15.75	64.39	1.5	15.25	0.3	0.01	0.175	0.475	0.65	0.5	1	-	-	-	2.33
Inconel 600	15.5	75.425	8	-	-	0.075	0.25	0.25	0.5	-	-	-	-	-	2.34
Hastelloy B3	1.5	63.595	1.5	28.5	0.25	0.005	-	0.05	1.5	1.5	1.5	0.1	-	-	2.35
Haynes 242	8	63.435	1	25	0.25	0.015	0.25	0.4	0.4	-	1.25	-	-	-	2.35
Hastelloy X	22	47.8	18	9	-	0.1	-	0.5	0.5	0.6	1.5	-	-	-	2.35
Haynes 188	22	22	1.5	-	-	0.1	-	0.35	0.625	14	39.425	-	-	-	2.35
Inconel 617	22	52.2	1.5	9	1.15	0.1	0.25	0.5	0.5	-	12.5	0.3	-	-	2.35
Haynes 230	22	56.7	1.5	2	0.3	0.1	-	0.4	0.5	14	2.5	-	-	-	2.35
Sanicro 28	27	32.03	34.705	3.5	-	0.015	1	0.5	1.25	-	-	-	-	-	2.35
Inconel 625	21.5	61.9	2.5	9	0.2	0.05	-	0.25	0.25	-	0.5	0.2	3.65	-	2.35
Incoloy 825 (2)	24.63	39.47	32.1	3.19	-	-	-	-	0.498	-	-	0.112	-	-	2.35
SS 310N	26	23	47.55	-	-	0.1	-	0.75	2	-	-	-	0.6	-	2.37
SS 316H	17	12	65.68	2.5	-	0.07	-	0.75	2	-	-	-	-	-	2.39
SS 304L	19	10	69.485	-	-	0.015	-	0.5	1	-	-	-	-	-	2.43
SS 316	17	12	66.96	2.5	-	0.04	-	0.5	1	-	-	-	-	-	2.43
Nimonic 90	19.5	56.585	0.75	-	1.5	0.065	0.1	0.5	0.5	-	18	2.5	-	-	2.44
SS 347H	18.5	11	68.27	-	-	0.07	-	0.5	1	-	-	-	0.66	-	2.45
Hastelloy B	0.5	63.925	5	28	-	0.025	-	0.5	0.5	-	1.25	-	-	0.3	2.46
Inconel 690	29	60.975	9	-	-	0.025	0.5	0.25	0.25	-	-	-	-	-	2.48
Haynes HR160	28	34.95	1.75	0.5	-	0.05	-	2.75	0.5	0.5	30	0.5	0.5	-	2.48
SS 317L	19	13	62.985	3.5	-	0.015	-	0.5	1	-	-	-	-	-	2.49
OC4	13.96	25.03	51.759	1.98	3.55	0.101	0.51	0.14	1.97	0.95	-	0.05	-	-	2.51

Alloy	Cr	Ni	Fe	Mo	Al	C	Cu	Si	Mn	W	Co	Ti	Nb	V	S_i
SS 353MA	25	35	38.565	-	-	0.035	-	0.65	0.75	-	-	-	-	-	2.51
Incoloy 800H	21	32.5	45.675	-	0.375	0.075	-	-	-	-	-	0.375	-	-	2.57
Inconel X750	15.5	71.81	7	-	0.7	0.04	0.25	0.25	0.5	-	0.5	2.5	0.95	-	2.59
Incoloy 800	21	32.5	45.7	-	0.375	0.05	-	-	-	-	-	0.375	-	-	2.67
SS 310	25	20.5	52.625	-	-	0.125	-	0.75	1	-	-	-	-	-	2.71
SS 347	17	11	69.66	-	-	0.04	-	0.5	1	-	-	-	0.8	-	2.73
SS 446	25	0.125	73.525	-	-	0.1	-	0.5	0.75	-	-	-	-	-	2.73
Inconel 686	21	57.745	1	16	-	0.005	-	0.04	0.375	3.7	-	0.135	-	-	2.75
SS HP40	26	35	33.45	0.5	-	0.55	-	2.5	2	-	-	-	-	-	2.76
SS 316L	17	12	66.985	2.5	-	0.015	-	0.5	1	-	-	-	-	-	2.77
SS 304	19	9.25	70.21	-	-	0.04	-	0.5	1	-	-	-	-	-	2.79
20#steel	0.125	0.125	98.65	-	-	0.205	0.125	0.27	0.5	-	-	-	-	-	2.81
Haynes HR120	25	35.85	33	1.25	0.1	0.05	-	0.6	0.7	1.25	1.5	-	0.7	-	2.87
SS 316Ti	17	12	66.735	2.5	-	0.04	-	0.375	1	-	-	0.35	-	-	2.87
Kaeri Super alloy 5	29	32	38.485	-	-	0.015	-	0.25	0.25	-	-	-	-	-	2.9
SS 405	13	-	85.76	-	0.2	0.04	-	0.5	0.5	-	-	-	-	-	2.91
SS 410	12.5	-	86.425	-	-	0.075	-	0.5	0.5	-	-	-	-	-	2.93
SS 1020	-	-	99.345	-	-	0.205	-	-	0.45	-	-	-	-	-	2.94
AlCoCrFeNi	20.6	23.3	22.1	-	10.7	-	-	-	-	-	23.3	-	-	-	2.95
SS 321	18	10.5	69.56	-	-	0.04	-	0.5	1	-	-	0.4	-	-	2.97
L 605	20	10	1.5	-	-	0.1	-	0.2	1.5	15	51.7	-	-	-	2.98
Nippon HR6W	24.5	34.35	30	-	-	0.1	-	1	1.5	8	-	0.2	0.35	-	3.02
SS 709	19.93	24.98	51.864	1.51	-	0.066	-	0.44	0.91	-	-	0.04	0.26	-	3.02
Haynes 556	22	20	32.8	3	0.2	0.1	-	0.4	1	2.5	18	-	-	-	3.07
SS 317	19	13	62.96	3.5	-	0.04	-	0.5	1	-	-	-	-	-	3.08

Alloy	Cr	Ni	Fe	Mo	Al	C	Cu	Si	Mn	W	Co	Ti	Nb	V	S_i
SS 15 15Ti	15.5	15.5	64.23	1.4	0.02	0.12	0.05	0.6	2	-	0.03	0.55	-	-	3.11
Nitronic 50	22	12.5	57.32	2.25	-	0.03	-	0.5	5	-	-	-	0.2	0.2	3.12
OCT	14	35	46	-	3	-	-	-	-	-	-	2	-	-	3.14
SS 321H	17	10.5	70.63	-	-	0.07	-	0.5	1	-	-	0.3	-	-	3.16
SS 330	19	36	43.395	-	-	0.04	-	0.565	1	-	-	-	-	-	3.24
Vuelvas 7	28.7	1.81	57.17	1.04	-	3.93	-	0.28	6.5	-	-	-	-	0.57	3.25
SS 430	14.94	-	84	-	-	0.06	-	0.5	0.5	-	-	-	-	-	3.33
SS 1045	-	-	98.79	-	-	0.46	-	-	0.75	-	-	-	-	-	3.37
X20	11.25	0.55	85.705	1	0.02	0.2	0.15	0.2	0.65	-	-	-	-	0.275	3.38
P91	8.75	0.2	88.89	0.95	0.01	0.1	-	0.35	0.45	-	-	0.005	0.08	0.215	3.39
Inconel 740H	24.5	49.1075	1.5	1	1.1	0.0425	0.25	0.5	0.5	-	18.5	1.5	1.5	-	3.40
$Cr_{18}Mn_{27}Fe_{27.5}Ni_{27.5}$	18	27.5	27.5	-	-	-	-	-	27	-	-	-	-	-	3.41
16Kh12MVSFBR	11	0.65	84.39	0.75	-	0.16	-	1.15	0.65	0.65	-	-	0.3	0.3	3.43
Vuelvas 1	21	1.58	62.59	2.2	-	5.17	-	0.34	6.27	-	-	-	-	0.85	3.44
T22	2.25	-	95.7	1	-	0.1	-	0.5	0.45	-	-	-	-	-	3.44
T23	2.25	-	94.99	0.175	0.015	0.07	-	0.25	0.35	1.6	-	-	0.05	0.25	3.47
SS 253MA	21	0.17	65.655	11	-	0.075	-	1.7	0.4	-	-	-	-	-	3.48
T9	9	-	88.85	1	-	0.075	-	0.625	0.45	-	-	-	-	-	3.5
SS4130	0.95	-	97.82	0.2	-	0.305	-	0.225	0.5	-	-	-	-	-	3.5
VM12	11.5	0.25	83.95	0.3	-	0.1	-	0.5	0.3	1.5	1.6	-	-	-	3.53
Vuelvas 6	27.7	1.86	56.65	0.98	-	3.93	-	0.32	7.42	-	-	-	-	1.14	3.59
T 11	1.2	-	96.97	0.5	-	0.1	-	0.79	0.44	-	-	-	-	-	3.61
Vuelvas 2	21.2	1.8	64.7	0.92	-	5.09	-	0.32	5.1	-	-	-	-	0.87	3.64
SS 439	18	0.25	80.64	-	0.075	0.035	-	0.5	0.5	-	-	-	-	-	3.64
SS Q235A	-	-	99.015	-	-	0.11	-	0.175	0.7	-	-	-	-	-	3.73

Alloy	Cr	Ni	Fe	Mo	Al	C	Cu	Si	Mn	W	Co	Ti	Nb	V	S_i
T92	8.75	0.2	88.015	0.45	0.02	0.1	-	0.5	0.45	1.25	-	-	0.065	0.2	3.74
A516	-	-	98.39	-	-	0.31	-	0.275	1.025	-	-	-	-	-	3.74
OCI	14	12	63.5	-	2.5	-	3	-	5	-	-	-	-	-	3.9
T24	2.4	-	95.36	1	0.01	0.1	-	0.3	0.5	-	-	0.08	-	0.25	3.91
Vuelvas 5	29.7	1.94	53.85	3.25	-	4.1	-	0.4	5.6	-	-	-	-	1.16	3.92
A1	-	-	98.7	-	-	0.27	-	0.1	0.93	-	-	-	-	-	3.97
Vuelvas 3	22.52	1.68	62.945	2.47	-	4.65	-	0.32	4.8	-	-	-	-	0.615	4.13
T5	5	-	93.85	0.55	-	0.075	-	0.075	0.45	-	-	-	-	-	4.16
T12	0.15	0.15	98.265	0.3	-	0.16	0.15	0.175	0.65	-	-	-	-	-	4.27
Vuelvas 4	30.48	1.96	53.12	3.3	-	4.29	-	0.42	5.9	-	-	-	-	0.53	4.31
SB450	-	-	99.045	-	-	0.28	-	0.225	0.45	-	-	-	-	-	4.44

Appendix B. Ranking of the Alloys Tested Under Wear Experiments

Alloy	Fe	C	Cr	Mn	Mo	V	W	Co	Ni	B	Nb	Si	N	Rank
Yoo-0,6B	76.6	1.73	19.94	-	-	-	-	-	-	0.71	-	1.02	-	1
Yoo-0,3B	77.7	1.74	19.32	-	-	-	-	-	-	0.34	-	0.9	-	2
Alloy S3/S21 (70/30)	0.93	1.76	29.45	0.52	1.65	-	8.75	53.24	2.08	0.7	-	0.93	-	3
Colmonoy 88	3.95	0.84	14.8	-	-	-	17.37	-	55.95	3.18	-	3.91	-	4
APM 2311	70.5	2	26	0.5	-	-	-	-	-	-	-	1	-	5
Stellite 12	2	1.8	29	-	-	-	8.5	54.20	3	-	-	1.5	-	6
Tribaloy T400	-	0.1	8.5	-	28.5	-	-	60.30	-	-	-	2.6	-	7
Yoo-1B	76.64	1.72	19.65	-	-	-	-	-	-	1.05	-	0.94	-	8
Colmonoy 6 Laser	3.8	0.73	14.56	-	-	-	-	0.09	73.17	3.37	-	4.28	-	9
Yoo-2B	75.82	1.72	19.54	-	-	-	-	-	-	2	-	0.92	-	10
NOREM A	56.9	1.2	26	5.5	2	-	-	-	5	-	-	3.4	-	11

Alloy	Fe	C	Cr	Mn	Mo	V	W	Co	Ni	B	Nb	Si	N	Rank
Elmax	76.6	1.7	17	0.3	1	3	-	-	-	-	-	0.4	-	12
Colmonoy 83	1.4	2	20	-	-	-	34	-	40.2	1	-	1.4	-	13
Tristelle TS-2	36	2	35	-	-	-	-	12	10	-	-	5	-	14
NOREM 02	59.7	1.23	25.1	4.4	2.03	-	-	-	4.13	-	-	3.23	0.18	15
Nelsit	59.97	0.03	18	2	3	-	-	-	10	-	-	7	-	16
Stellite 21	3	0.25	27	1	5.5	-	-	59.25	2.5	-	-	1.5	-	17
NOREM 01	55.28	1	25	9.3	2	-	-	-	4.02	-	-	3.3	0.1	18
Stellite 6	2.01	1.2	29	0.13	1.5	-	4.5	59.02	1.8	-	-	0.84	-	19
Yoo-0B	77.03	1.64	20.34	-	-	-	-	-	-	0.01	-	0.98	-	20
NOREM 04	46.73	1.05	24.81	12	1.96	-	-	-	8.05	-	-	5.17	0.23	21
AI 1236	2.86	1.58	9.56	-	-	-	25.92	-	55.13	2.15	-	2.8	-	22
Tribaloy T200	-	-	11	-	-	-	-	61.75	20	-	6.5	0.75	-	23
NoCo-M2	55.95	0.9	25	5	2	-	-	-	8	-	-	3	0.15	24
Everit 50	67.7	2	25	0.9	3.5	0.5	-	-	-	-	-	0.4	-	25
Colmonoy 5	4.6	0.5	12.6	-	-	-	-	-	75.8	2.5	-	4	-	26
Nucalloy 453	3	0.85	10	-	-	-	2	-	78.35	0.5	-	5.3	-	27
Tribaloy T700	-	0.08	16	-	32	-	-	1.5	47.02	-	-	3.4	-	28
Deloro 40	2.5	0.45	10	-	-	-	-	-	82.25	2.5	-	2.3	-	29
Deloro 50	4	0.6	13	-	-	-	-	-	75.4	3	-	4	-	30
Inconel 625	1	0.05	21		9	-	-	-	68.95	-	-	-	-	31
Nucalloy 488	5.5	0.3	17.5	-	-	-	1	-	67.9	1	-	6.8	-	32
Tribaloy T700 + 10% Fe	10	0.08	16	-	32	-	-	1.5	35.02	-	-	5.4	-	33
Tribaloy T700 + 5% Fe	5	0.08	16	-	32	-	-	1.5	41.02	-	-	4.4	-	34
Tribaloy T700 + 15% Fe	15	0.08	16	-	32	-	-	1.5	29.02	-	-	6.4	-	35

References

1. Ramprasad, R.; Batra, R.; Pilania, G.; Mannodi-Kanakkithodi, A.; Kim, C. Machine learning in materials informatics: Recent applications and prospects. *Npj Comput. Mater.* **2017**, *3*, 54. [CrossRef]
2. Vasudevan, R.; Pilania, G.; Balachandran, P.V. Machine learning for materials design and discovery. *J. Appl. Phys.* **2021**, *129*, 070401. [CrossRef]
3. Bhadeshia, H.K.D.H. Neural networks in materials science. *ISIJ Int.* **1999**, *39*, 966–979. [CrossRef]
4. Bailer-Jones, C.; Bhadeshia, H.; MacKay, D. Gaussian process modelling of austenite formation in steel. *Mater. Sci. Technol.* **1999**, *15*, 287–294. [CrossRef]
5. Pei, J.; Cai, C.; Zhu, X.; Wang, G. Investigation on the Processing-Properties of Hot Deformed TA15 Titanium Alloy via Support Vector Regression. *Mater. Sci. Forum* **2011**, *689*, 134–143. [CrossRef]
6. Jha, R.; Pettersson, F.; Dulikravich, G.S.; Saxen, H.; Chakraborti, N. Evolutionary Design of Nickel-Based Superalloys Using Data-Driven Genetic Algorithms and Related Strategies. *Mater. Manuf. Process.* **2014**, *30*, 488–510. [CrossRef]
7. Tancret, F. Materials Design: Computational Alloy Design by Combinatorial Optimization. In *Encyclopedia of Materials: Metals and Alloys*; Elsevier: Amsterdam, The Netherlands, 2022; pp. 596–608.
8. Menon, D.; Ranganathan, R. A Generative Approach to Materials Discovery, Design, and Optimization. *ACS Omega* **2022**, *7*, 25958–25973. [CrossRef] [PubMed]
9. Rajan, K. Materials informatics. *Mater. Today* **2005**, *8*, 38–45. [CrossRef]
10. Li, C.; Zheng, K. Methods, progresses, and opportunities of materials informatics. *InfoMat* **2023**, *5*, e12425. [CrossRef]
11. Saal, J.E.; Kirklin, S.; Aykol, M.; Meredig, B.; Wolverton, C. Materials Design and Discovery with High-Throughput Density Functional Theory: The Open Quantum Materials Database (OQMD). *JOM* **2013**, *65*, 1501–1509. [CrossRef]
12. Jain, A.; Ong, S.P.; Hautier, G.; Chen, W.; Richards, W.D.; Dacek, S.; Cholia, S.; Gunter, D.; Skinner, D.; Ceder, G.; et al. Commentary: The Materials Project: A materials genome approach to accelerating materials innovation. *APL Mater.* **2013**, *1*, 011002. [CrossRef]
13. de Pablo, J.J.; Jones, B.; Kovacs, C.L.; Ozolins, V.; Ramirez, A.P. The Materials Genome Initiative, the interplay of experiment, theory and computation. *Curr. Opin. Solid State Mater. Sci.* **2014**, *18*, 99–117. [CrossRef]
14. Garel, E.; Parouty, J.-L.; Van Landeghem, H.; Verdier, M.; Robaut, F.; Coindeau, S.; Boichot, R. Coupling mixture designs, high-throughput experiments and machine learning for accelerated exploration of multinary systems. *Mater. Des.* **2023**, *231*, 112055. [CrossRef]
15. Si, S.; Fan, B.; Liu, X.; Zhou, T.; He, C.; Song, D.; Liu, J. Study on strengthening effects of Zr-Ti-Nb-O alloys via high throughput powder metallurgy and data-driven machine learning. *Mater. Des.* **2021**, *206*, 109777. [CrossRef]
16. Muránsky, O.; Yang, C.; Zhu, H.; Karatchevtseva, I.; Sláma, P.; Nový, Z.; Edwards, L. Molten salt corrosion of Ni-Mo-Cr candidate structural materials for Molten Salt Reactor (MSR) systems. *Corros. Sci.* **2019**, *159*, 108087. [CrossRef]
17. Sankar, K.M.; Keiser, J.R.; Sulejmanovic, D.; Lowe, T.M.; Singh, P.M. Evaluation of Corrosion Behavior of Various Fe-and Ni-Based Alloys in Molten Li2BeF4 (FLiBe). *Nucl. Technol.* **2023**, *210*, 391–408. [CrossRef]
18. Sun, H.; Wang, J.; Li, Z.; Zhang, P.; Su, X. Corrosion behavior of 316SS and Ni-based alloys in a ternary NaCl-KCl-$MgCl_2$ molten salt. *Sol. Energy* **2018**, *171*, 320–329. [CrossRef]
19. Dorcheh, A.S.; Durham, R.N.; Galetz, M.C. Corrosion behavior of stainless and low-chromium steels and IN625 in molten nitrate salts at 600 °C. *Sol. Energy Mater. Sol. Cells* **2016**, *144*, 109–116. [CrossRef]
20. De Bacco, C.; Larremore, D.B.; Moore, C. A physical model for efficient ranking in networks. *Sci. Adv.* **2018**, *4*, eaar8260. [CrossRef]
21. Lee, E.; Clauset, A.; Larremore, D.B. The dynamics of faculty hiring networks. *EPJ Data Sci.* **2021**, *10*, 48. [CrossRef]
22. Wapman, K.H.; Zhang, S.; Clauset, A.; Larremore, D.B. Quantifying hierarchy and dynamics in US faculty hiring and retention. *Nature* **2022**, *610*, 120–127. [CrossRef] [PubMed]
23. Rateau, L. Conception et Caractérisation d'Alliages Métalliques Durs pour des Applications de Résistance à l'usure. Ph.D. Thesis, Université de Nantes, Nantes, France, 2023.
24. Kichikawa, Y.; Iino, T.; Iyetomi, H.; Inoue, H. Hierarchical and Circular Flow Structure of the Interfirm Transaction Network in Japan. *Appl. Netw. Sci.* **2019**, *4*, 1–23. [CrossRef]
25. Rasmussen, C.E.; Williams, C.K.I. *Gaussian Processes for Machine Learning*; MIT Press: Cambridge, MA, USA, 2005. [CrossRef]
26. Tancret, F.; Bhadeshia, H.K.D.H.; Mackay, D.J.C. Comparison of Artificial Neural Networks with Gaussian Processes to Model the Yield Strength of Nickel-Base Superalloys. *ISIJ Int.* **1999**, *39*, 1020–1026. [CrossRef]
27. Tancret, F.; Toda-Caraballo, I.; Menou, E.; Díaz-Del-Castillo, P.E.J.R. Designing high entropy alloys employing thermodynamics and Gaussian process statistical analysis. *Mater. Des.* **2017**, *115*, 486–497. [CrossRef]
28. Assi, M.; Favre, J.; Fraczkiewicz, A.; Tancret, F. Machine learning-based model of surface tension of liquid metals: A step in designing multicomponent alloys for additive manufacturing. *J. Mater. Sci.* **2022**, *57*, 13446–13466. [CrossRef]
29. Deb, K.; Pratap, A.; Agarwal, S.; Meyarivan, T. A fast and elitist multiobjective genetic algorithm: NSGA-II. *IEEE Trans. Evol. Comput.* **2002**, *6*, 182–197. [CrossRef]
30. Menou, E.; Ramstein, G.; Bertrand, E.; Tancret, F. Multi-objective constrained design of nickel-base superalloys using data mining- and thermodynamics-driven genetic algorithms. *Model. Simul. Mater. Sci. Eng.* **2016**, *24*, 055001. [CrossRef]
31. Menou, E.; Tancret, F.; Toda-Caraballo, I.; Ramstein, G.; Castany, P.; Bertrand, E.; Gautier, N.; Díaz-Del-Castillo, P.E.J.R. Computational design of light and strong high entropy alloys (HEA): Obtainment of an extremely high specific solid solution hardening. *Scr. Mater.* **2018**, *156*, 120–123. [CrossRef]

32. Serp, J.; Allibert, M.; Beneš, O.; Delpech, S.; Feynberg, O.; Ghetta, V.; Heuer, D.; Holcomb, D.; Ignatiev, V.; Kloosterman, J.L.; et al. The molten salt reactor (MSR) in generation IV: Overview and perspectives. *Prog. Nucl. Energy* **2014**, *77*, 308–319. [CrossRef]
33. LeBlanc, D. Molten salt reactors: A new beginning for an old idea. *Nucl. Eng. Des.* **2010**, *240*, 1644–1656. [CrossRef]
34. Mausolff, Z.; DeHart, M.; Goluoglu, S. Design and assessment of a molten chloride fast reactor. *Nucl. Eng. Des.* **2021**, *379*, 111181. [CrossRef]
35. Wright, R.N.; Sham, T.L. *Status of Metallic Structural Materials for Molten Salt Reactors*; Report No.: INL/EXT-18-45171-Rev000; Idaho National Lab (INL): Idaho Falls, ID, USA; Argonne National Lab (ANL): Argonne, IL, USA, 2018.
36. Roper, R.; Harkema, M.; Sabharwall, P.; Riddle, C.; Chisholm, B.; Day, B.; Marotta, P. Molten salt for advanced energy applications: A review. *Ann. Nucl. Energy* **2022**, *169*, 108924. [CrossRef]
37. Meißner, T.M.; Oskay, C.; Bonk, A.; Grégoire, B.; Donchev, A.; Solimani, A.; Galetz, M.C. Improving the corrosion resistance of ferritic-martensitic steels at 600 °C in molten solar salt via diffusion coatings. *Sol. Energy Mater. Sol. Cells* **2021**, *227*, 111105. [CrossRef]
38. Dorcheh, A.S.; Durham, R.N.; Galetz, M.C. High temperature corrosion in molten solar salt: The role of chloride impurities. *Mater. Corros.* **2017**, *68*, 943–951. [CrossRef]
39. Cho, S.H.; Bin Park, S.; Lee, J.H.; Hur, J.M.; Lee, H.S. Corrosion behavior of Ni-based structural materials for electrolytic reduction in lithium molten salt. *J. Nucl. Mater.* **2011**, *412*, 157–164. [CrossRef]
40. Bonk, A.; Rückle, D.; Kaesche, S.; Braun, M.; Bauer, T. Impact of Solar Salt aging on corrosion of martensitic and austenitic steel for concentrating solar power plants. *Sol. Energy Mater. Sol. Cells* **2019**, *203*, 110162. [CrossRef]
41. Bell, S.; Jones, M.; Graham, E.; Peterson, D.; van Riessen, G.; Hinsley, G.; Steinberg, T.; Will, G. Corrosion mechanism of SS316L exposed to NaCl/Na2CO3 molten salt in air and argon environments. *Corros. Sci.* **2022**, *195*, 109966. [CrossRef]
42. Wang, J.; Jiang, Y.; Ni, Y.; Wu, A.; Li, J. Investigation on static and dynamic corrosion behaviors of thermal energy transfer and storage system materials by molten salts in concentrating solar power plants. *Mater. Corros.* **2018**, *70*, 102–109. [CrossRef]
43. Pedrosa, F.; Paiva, T.; Figueira, I.; Diamantino, T.C. Hight-temperatures corrosion of AISI 316L and AISI 430 steels in dynamic conditions with molten salar salt. *8as Jorn. De Corrosão E Proteção De Mater.* **2022**, 39–41. [CrossRef]
44. Olson, L.C.; Fuentes, R.E.; Martinez-Rodriguez, M.J.; Ambrosek, J.W.; Sridharan, K.; Anderson, M.H.; Garcia-Diaz, B.L.; Gray, J.; Allen, T.R. Impact of Corrosion Test Container Material in Molten Salt. *J. Sol. Energy Eng.* **2015**, *137*, 061007. [CrossRef]
45. Pavlík, V.; Boča, M.; Kityk, A. Accelerated corrosion testing in molten fluoride salts: Effect of additives and the crucible material. *Corros. Sci.* **2022**, *195*, 110011. [CrossRef]
46. Liu, Q.; Qian, J.; Neville, A.; Pessu, F. Solar thermal irradiation cycles and their influence on the corrosion behaviour of stainless steels with molten salt used in concentrated solar power plants. *Sol. Energy Mater. Sol. Cells* **2022**, *251*, 112141. [CrossRef]
47. Wang, Y.; Zeng, C.; Li, W. The influence of temperature gradient on the corrosion of materials in molten fluorides. *Corros. Sci.* **2018**, *136*, 180–187. [CrossRef]
48. Feng, J.; Mao, L.; Yuan, G.; Zhao, Y.; Vidal, J.; Liu, L. Grain size effect on corrosion behavior of Inconel 625 film against molten $MgCl_2$-NaCl-KCl salt. *Corros. Sci.* **2022**, *197*, 110097. [CrossRef]
49. Li, X.; Chang, L.; Liu, C.; Leng, B.; Ye, X.; Han, F.; Yang, X. Effect of thermal aging on corrosion behavior of type 316H stainless steel in molten chloride salt. *Corros. Sci.* **2021**, *191*, 109784. [CrossRef]
50. Sarvghad, M.; Chenu, T.; Will, G. Comparative interaction of cold-worked versus annealed inconel 601 with molten carbonate salt at 450°C. *Corros. Sci.* **2017**, *116*, 88–97. [CrossRef]
51. Kondaiah, P.; Pitchumani, R. Fractal textured surfaces for high temperature corrosion mitigation in molten salts. *Sol. Energy Mater. Sol. Cells* **2021**, *230*, 111281. [CrossRef]
52. Wang, Y.L.; Wang, Q.; Liu, H.J.; Zeng, C.L. The effect of the microstructure on the corrosion behavior of N5 superalloy in a molten (Li,Na,K)F eutectic salt. *RSC Adv.* **2015**, *5*, 32755–32760. [CrossRef]
53. Wei, B.; Chen, C.; Xu, J.; Yang, L.; Jia, Y.; Du, Y.; Guo, M.; Sun, C.; Wang, Z.; Wang, F. Comparing the hot corrosion of (100), (210) and (110) Ni-based superalloys exposed to the mixed salt of Na2SO4-NaCl at 750 °C: Experimental study and first-principles calculation. *Corros. Sci.* **2022**, *195*, 109996. [CrossRef]
54. Vuelvas-Rayo, S.; Gonzalez-Rodriguez, J.G.; Porcayo-Calderon, J.; Salinas-Bravo, V.M. Hot Corrosion Behavior of High-Chromium, High-Carbon Cast Irons in NaCl-KCl Molten Salts. *Int. J. Corros.* **2012**, *2012*, 479761. [CrossRef]
55. Fernández, A.G.; Cabeza, L.F. Anodic Protection Assessment Using Alumina-Forming Alloys in Chloride Molten Salt for CSP Plants. *Coatings* **2020**, *10*, 138. [CrossRef]
56. Cho, S.H.; Hong, S.S.; Kang, D.S.; Hur, J.M.; Lee, H.S. Hot Corrosion Behavior of Ni-Base Superalloys in a Lithium Molten Salt. *Met. Mater. Int.* **2009**, *15*, 51–55. [CrossRef]
57. Sulejmanovic, D.; Kurley, J.M.; Robb, K.; Raiman, S. Validating modern methods for impurity analysis in fluoride salts. *J. Nucl. Mater.* **2021**, *553*, 152972. [CrossRef]
58. Williams, T.; Shum, R.; Rappleye, D. Review—Concentration Measurements In Molten Chloride Salts Using Electrochemical Methods. *J. Electrochem. Soc.* **2021**, *168*, 123510. [CrossRef]
59. Ozdemir, H.; Nazarahari, A.; Yilmaz, B.; Canadinc, D.; Bedir, E.; Yilmaz, R.; Unal, U.; Maier, H. Machine learning—informed development of high entropy alloys with enhanced corrosion resistance. *Electrochim. Acta* **2023**, *476*, 143722. [CrossRef]
60. Roy, A.; Taufique, M.F.N.; Khakurel, H.; Devanathan, R.; Johnson, D.D.; Balasubramanian, G. Machine-learning-guided descriptor selection for predicting corrosion resistance in multi-principal element alloys. *Npj Mater. Degrad.* **2022**, *6*, 9. [CrossRef]

61. Sasidhar, K.N.; Siboni, N.H.; Mianroodi, J.R.; Rohwerder, M.; Neugebauer, J.; Raabe, D. Enhancing corrosion-resistant alloy design through natural language processing and deep learning. *Sci. Adv.* **2023**, *9*, eadg7992. [CrossRef]
62. Sasidhar, K.N.; Siboni, N.H.; Mianroodi, J.R.; Rohwerder, M.; Neugebauer, J.; Raabe, D. Deep learning framework for uncovering compositional and environmental contributions to pitting resistance in passivating alloys. *Npj Mater. Degrad.* **2022**, *6*, 71. [CrossRef]
63. Wang, Y.; Goh, B.; Nelaturu, P.; Duong, T.; Hassan, N.; David, R.; Moorehead, M.; Chaudhuri, S.; Creuziger, A.; Hattrick-Simpers, J.; et al. Integrated High-Throughput and Machine Learning Methods to Accelerate Discovery of Molten Salt Corrosion-Resistant Alloys. *Adv. Sci.* **2022**, *9*, 2200370. [CrossRef]
64. Raiman, S.S.; Lee, S. Aggregation and data analysis of corrosion studies in molten chloride and fluoride salts. *J. Nucl. Mater.* **2018**, *511*, 523–535. [CrossRef]
65. Sankar, K.M.; Singh, P.M. Effect of metal fluorides on the corrosion of structural materials in molten LiF-NaF-KF. *Corros. Sci.* **2023**, *213*, 110977. [CrossRef]
66. Sawant, S.; Gajbhiye, B.; Tyagi, S.; Sona, C.; Divya, R.; Mathpati, C.; Borgohain, A.; Maheshwari, N. High Temperature Corrosion Studies in Molten Salt Using Salt Purification and Alloy Coating. *Indian Chem. Eng.* **2016**, *59*, 242–257. [CrossRef]
67. Elbakhshwan, M.; Doniger, W.; Falconer, C.; Moorehead, M.; Parkin, C.; Zhang, C.; Sridharan, K.; Couet, A. Corrosion and Thermal Stability of CrMnFeNi High Entropy Alloy in Molten FLiBe Salt. *Sci. Rep.* **2019**, *9*, 18993. [CrossRef] [PubMed]
68. Fernández, A.; Cortes, M.; Fuentealba, E.; Pérez, F. Corrosion properties of a ternary nitrate/nitrite molten salt in concentrated solar technology. *Renew. Energy* **2015**, *80*, 177–183. [CrossRef]
69. Fernández, A.G.; Rey, A.; Lasanta, I.; Mato, S.; Brady, M.P.; Pérez, F.J. Corrosion of alumina-forming austenitic steel in molten nitrate salts by gravimetric analysis and impedance spectroscopy. *Mater. Corros.* **2014**, *65*, 267–275. [CrossRef]
70. Fernández, A.; Galleguillos, H.; Fuentealba, E.; Pérez, F. Corrosion of stainless steels and low-Cr steel in molten $Ca(NO_3)_2$–$NaNO_3$–KNO_3 eutectic salt for direct energy storage in CSP plants. *Sol. Energy Mater. Sol. Cells* **2015**, *141*, 7–13. [CrossRef]
71. Mallco, A.; Portillo, C.; Kogan, M.J.; Galleguillos, F.; Fernández, A.G. A Materials Screening Test of Corrosion Monitoring in $LiNO_3$ Containing Molten Salts as a Thermal Energy Storage Material for CSP Plants. *Appl. Sci.* **2020**, *10*, 3160. [CrossRef]
72. Suzuki, Y.; Watanabe, T.; Goto, T. Electrochemical and spectroscopic study on corrosion behavior of Ni-based alloys in chloride melts: Materials for an integral molten salt fast reactor. *Nucl. Eng. Des.* **2023**, *415*, 112699. [CrossRef]
73. Karpov, V.A.; Abramov, A.V.; Dedov, K.V.; Shak, A.V.; Zhilyakov, A.Y.; Polovov, I.B.; Polovov, I.B.; Belikov, S.V.; Rebrin, O.I. Corrosion of Various Types of Stainless Steel in Chloroaluminate Melts. *Russ. Metall. Met.* **2019**, *2019*, 190–193. [CrossRef]
74. Gomez-Vidal, J.C.; Tirawat, R. Corrosion of alloys in a chloride molten salt (NaCl-LiCl) for solar thermal technologies. *Sol. Energy Mater. Sol. Cells* **2016**, *157*, 234–244. [CrossRef]
75. Liu, B.; Wei, X.; Wang, W.; Lu, J.; Ding, J. Corrosion behavior of Ni-based alloys in molten NaCl-$CaCl_2$-$MgCl_2$ eutectic salt for concentrating solar power. *Sol. Energy Mater. Sol. Cells* **2017**, *170*, 77–86. [CrossRef]
76. Banerjee, R.H.; Singh, V.; Arya, A.; Banerjee, S. A comparative study of surface layer formation in Ni-based alloys with varying Cr contents exposed to high temperature fluoride environment. *J. Nucl. Mater.* **2019**, *516*, 54–62. [CrossRef]
77. Abramov, A.V.; Polovov, I.B.; Volkovich, V.A.; Rebrin, O.I.; Denisov, E.I.; Griffiths, T.R. Corrosion of Austenitic Steels and Their Components in Vanadium-Containing Chloride Melts. *ECS Trans.* **2013**, *50*, 685–698. [CrossRef]
78. Zhang, J.; Rahman, Z.U.; Wang, X.; Wang, Z.; Li, P.; Wang, Y.; Bate, D.; Zhao, K.; Tan, H. Hot corrosion behaviors of TP347H and HR3C stainless steel with KCl deposit in oxy-biomass combustion. *J. Environ. Manag.* **2020**, *263*, 110411. [CrossRef] [PubMed]
79. Li, Y.S.; Niu, Y.; Wu, W.T. Accelerated corrosion of pure Fe, Ni, Cr and several Fe-based alloys induced by $ZnCl_2$-KCl at 450 °C in oxidizing environment. *Mater. Sci. Eng. A* **2003**, *345*, 64–71. [CrossRef]
80. Wang, C.-J.; Li, C.-C. The High-Temperature Corrosion of Austenitic Stainless Steel with a NaCl Deposit at 850 °C. *Oxid. Met.* **2004**, *61*, 485–505. [CrossRef]
81. Liu, T.; Xu, X.; Liu, W.; Zhuang, X. Corrosion of alloys in high temperature molten-salt heat transfer fluids with air as the cover gas. *Sol. Energy* **2019**, *191*, 435–448. [CrossRef]
82. Grantham, L.F.; Shaw, P.H.; Oldenkamp, R.D. Corrosion of Metals in Molten Mixtures of Alkali Metal Carbonates Containing Sulfur Compounds. In *High Temperature Metallic Corrosion of Sulfur and Its Compound*; University of California: Los Angeles, CA, USA, 1970.
83. Zhuang, X.; Liu, W.; Xu, X. Hot corrosion of different alloys in chloride and carbonate molten-salt mixtures under argon atmosphere. *Sol. Energy* **2019**, *189*, 254–267. [CrossRef]
84. Eriksson, J.-E.; Lehmusto, J.; Dirbeba, M.; Silvander, L.; Lindberg, D.; Hupa, L. The effect of Cl, Br, and F on high-temperature corrosion of heat-transfer alloys. *Fuel* **2023**, *348*, 128516. [CrossRef]
85. Pan, P.; Li, T.; Wang, Y.; Zhang, N.; Chen, H. Effect of temperature on hot corrosion of nickel-based alloys for 700 °C A-USC power plants. *Corros. Sci.* **2022**, *203*, 110350. [CrossRef]
86. Dudziak, T.; Hussain, T.; Orlicka, D.; Pokrywa, A.; Simms, N. Fireside corrosion degradation of 15Mo3, T22, T23 & T91 in simulated coal-biomass co-fired environment. *Mater. Corros.* **2015**, *66*, 839–850. [CrossRef]
87. Tsao, T.-K.; Yeh, A.-C.; Kuo, C.-M.; Murakami, H. High Temperature Oxidation and Corrosion Properties of High Entropy Superalloys. *Entropy* **2016**, *18*, 62. [CrossRef]
88. Men, D.; Xiong, J.; Peng, W.; Bai, L. Study on Molten Salt Corrosion Behavior of Several Stainless Steel Alloys. *J. Phys. Conf. Ser.* **2021**, *1885*, 032005. [CrossRef]

89. Abu-Warda, N.; López, A.J.; Pedraza, F.; Utrilla, M.V. Corrosion behavior of T24, T92, VM12, and AISI 304 steels exposed to KCl–NaCl–K2SO4–Na2SO4 salt mixtures. *Mater. Corros.* **2021**, *72*, 936–950. [CrossRef]
90. Sankar, K.M.; Singh, P.M. Effect of Li metal addition on corrosion control of Hastelloy N and stainless steel 316H in molten LiF-NaF-KF. *J. Nucl. Mater.* **2021**, *555*, 153098. [CrossRef]
91. Li, H.; Wang, X.; Yin, X.; Yang, X.; Tang, J.; Gong, J. Corrosion and electrochemical investigations for stainless steels in molten Solar Salt: The influence of chloride impurity. *J. Energy Storage* **2021**, *39*, 102675. [CrossRef]
92. Fernández, A.; Grágeda, M.; Galleguillos, H. Impurity Influence in Physico-chemical and Corrosion Properties of Chilean Solar Nitrates. *Energy Procedia* **2014**, *49*, 607–616. [CrossRef]
93. Wang, L.; Li, B.; Shen, M.; Li, S.; Yu, J. Corrosion resistance of steel materials in LiCl-KCl melts. *Int. J. Miner. Metall. Mater.* **2012**, *19*, 930–933. [CrossRef]
94. Rao, C.J.; Ningshen, S.; Mallika, C.; Mudali, U.K. Molten salt corrosion behavior of structural materials in LiCl-KCl-UCl3 by thermogravimetric study. *J. Nucl. Mater.* **2018**, *501*, 189–199. [CrossRef]
95. Ding, W.; Shi, H.; Xiu, Y.; Bonk, A.; Weisenburger, A.; Jianu, A.; Bauer, T. Hot corrosion behavior of commercial alloys in thermal energy storage material of molten $MgCl_2$/KCl/NaCl under inert atmosphere. *Sol. Energy Mater. Sol. Cells* **2018**, *184*, 22–30. [CrossRef]
96. Cho, S.H.; Zhang, J.S.; Shin, Y.J.; Park, S.W.; Park, H.S. Corrosion behavior of Fe–Ni–Cr alloys in the molten salt of LiCl–Li_2O at high temperature. *J. Nucl. Mater.* **2004**, *325*, 13–17. [CrossRef]
97. Palacios, A.; Navarro, M.E.; Jiang, Z.; Avila, A.; Qiao, G.; Mura, E.; Ding, Y. High-temperature corrosion behaviour of metal alloys in commercial molten salts. *Sol. Energy* **2020**, *201*, 437–452. [CrossRef]
98. Navarro, M.; Palacios, A.; Jiang, Z.; Avila, A.; Qiao, G.; Mura, E.; Ding, Y. Effect of SiO_2 nanoparticles concentration on the corrosion behaviour of solar salt-based nanofluids for Concentrating Solar Power plants. *Sol. Energy Mater. Sol. Cells* **2022**, *247*, 111923. [CrossRef]
99. Sah, S.P.; Tada, E.; Nishikata, A. Corrosion behaviour of austenitic stainless steels in carbonate melt at 923 K under controlled CO_2-O_2 environment. *Corros. Sci.* **2018**, *133*, 310–317. [CrossRef]
100. Cheng, W.J.; Chen, D.J.; Wang, C.J. High-temperature corrosion of Cr–Mo steel in molten LiNO3–NaNO3–KNO3 eutectic salt for thermal energy storage. *Sol. Energy Mater. Sol. Cells* **2015**, *132*, 563–569. [CrossRef]
101. Ruiz-Cabañas, F.J.; Jové, A.; Prieto, C.; Madina, V.; Fernández, A.I.; Cabeza, L.F. Materials selection of steam-phase change material (PCM) heat exchanger for thermal energy storage systems in direct steam generation facilities. *Sol. Energy Mater. Sol. Cells* **2017**, *159*, 526–535. [CrossRef]
102. Sona, C.B.; Gajbhiye, B.D.; Hule, P.V.; Patwardhan, A.W.; Mathpati, A.W.; Borgohain, A.; Maheshwari, N.K. High temperature corrosion studies in molten salt-FLiNaK. *Corros. Eng. Sci. Technol.* **2014**, *49*, 287–295. [CrossRef]
103. Kumar, M.P.; Manikandan, M. Insights into the surface behavior of Inconel 617 and Inconel 625 material in molten salt. *Mater. Lett.* **2022**, *333*, 133679. [CrossRef]
104. Vignarooban, K.; Xu, X.; Wang, K.; Molina, E.; Li, P.; Gervasio, D.; Kannan, A. Vapor pressure and corrosivity of ternary metal-chloride molten-salt based heat transfer fluids for use in concentrating solar power systems. *Appl. Energy* **2015**, *159*, 206–213. [CrossRef]
105. Zhai, W.; Yang, B.; Li, M.; Li, S.; Xin, M.; Zhang, S.; Huang, G. Study on Corrosion of Metal Materials in Nitrate Molten Salts. In Proceedings of the 2016 International Conference on Materials Science, ReSource and Environmental Engineering, Xi'an, China, 10–11 December 2016.
106. Barnett, R.; Gittos, M. High Temperature Corrosion of Nickel Alloys by Molten Calcium Chloride in an Oxidising Environment. In Proceedings of the International Conference on Water Chemistry of Nuclear Reactor Systems, Paris, France, 23–27 September 2012.
107. Mahajan, S.; Chhibber, R. Hot corrosion studies of boiler steels exposed to different molten salt mixtures at 950 °C. *Eng. Fail. Anal.* **2019**, *99*, 210–224. [CrossRef]
108. Olson, L.C.; Sridharan, K.; Anderson, M.H.; Allen, T.R. Intergranular corrosion of high temperature alloys in molten fluoride salts. *Mater. High Temp.* **2010**, *27*, 145–149. [CrossRef]
109. Liu, Q.; Qian, J.; Barker, R.; Wang, C.; Neville, A.; Pessu, F. Effect of thermal cycling on the corrosion behaviour of stainless steels and Ni-based alloys in molten salts under air and argon. *Sol. Energy* **2022**, *238*, 248–257. [CrossRef]
110. Sidhu, T.S.; Malik, A.; Prakash, S.; Agrawal, R.D. Cyclic oxidation behavior of Ni-and Fe-based superalloys in air and Na2SO4-25% NaCl molten salt environment at 800° C. *Int. J. Phys. Sci.* **2006**, *1*, 27–33.
111. Sutter, F.; Oskay, C.; Galetz, M.C.; Diamantino, T.; Pedrosa, F.; Figueira, I.; Glumm, S.; Bonk, A.; Agüero, A.; Rodríguez, S.; et al. Dynamic corrosion testing of metals in solar salt for concentrated solar power. *Sol. Energy Mater. Sol. Cells* **2021**, *232*, 111331. [CrossRef]
112. Alimgulov, R.R.; Abramov, A.V.; Karpov, V.V.; Maltsev, D.S.; Volkovich, V.A.; Polovov, I.B.; Rebrin, O.I. Corrosion of Construction Materials in KCl–LiCl–UCl3 Melts Containing Metallic Zinc. In Proceedings of the VI International Young Researchers' Conference, Ekaterinburg, Russia, 20–23 May 2019; Volume 2174, p. 020003.
113. Shankar, A.R.; Ravi, A.; Kanagasundar, A.; Mudali, U.K. Corrosion of Nickel-Containing Alloys in Molten LiCl-KCl. *Medium Corros.* **2013**, *69*, 48–57. [CrossRef]
114. Chang, S.; Jia, Y.; Du, X.; Guo, S. Corrosion Behavior of Commercial Alloys in LiCl–KCl Molten Salt Containing EuCl3. *Front. Mater.* **2022**, *9*, 958296. [CrossRef]

115. Wang, W.; Guan, B.; Li, X.; Lu, J.; Ding, J. Corrosion behavior and mechanism of austenitic stainless steels in a new quaternary molten salt for concentrating solar power. *Sol. Energy Mater. Sol. Cells* **2019**, *194*, 36–46. [CrossRef]
116. Goods, R.H.; Bradshaw, R.W. Corrosion of stainless steels and carbon steel by molten mixtures of commercial nitrate salts. *J. Mater. Eng. Perform.* **2004**, *13*, 78–87. [CrossRef]
117. Elbakhshwan, M.; Lee, D.H.; Anderson, M. Corrosion resistance of high nickel alloys in solar salt at 600 °C for up to 4000 h. *Sol. Energy Mater. Sol. Cells* **2022**, *245*, 111837. [CrossRef]
118. Polovov, I.B.; Abramov, A.V.; Karpov, V.V.; Gibadullina, A.F.; Zhilyakov, A.Y.; Dedov, K.V.; Belikov, S.V.; Shak, A.V.; Volkovich, V.A.; Rebrin, O.I. Corrosion of nickel-based superalloys in molten chloroaluminates. *ECS Trans.* **2017**, *77*, 753. [CrossRef]
119. Patel, K.; Sadeghilaridjani, M.; Pole, M.; Mukherjee, S. Hot corrosion behavior of refractory high entropy alloys in molten chloride salt for concentrating solar power systems. *Sol. Energy Mater. Sol. Cells* **2021**, *230*, 111222. [CrossRef]
120. Lim, J.H.; Jung, W.J. Corrosion Behavior of Superalloys in a LiCl-Li2O Molten Salt. *Mater. Trans.* **2014**, *55*, 1618–1622. [CrossRef]
121. Arteaga, C.C.; Sotelo-Mazón, O.; Rodríguez, J.A.; Clemente, C.M. Comparison of the corrosion performance of alloys HP40 and T22 exposed to molten salts at high temperature. *Mater. High Temp.* **2021**, *38*, 123–138. [CrossRef]
122. Pineda, F.; Walczak, M.; Vilchez, F.; Guerra, C.; Escobar, R.; Sancy, M. Evolution of corrosion products on ASTM A36 and AISI 304L steels formed in exposure to molten NaNO3–KNO3 eutectic salt: Electrochemical study. *Corros. Sci.* **2021**, *196*, 110047. [CrossRef]
123. Lee, M.; Muránsky, O.; Karatchevtseva, I.; Huang, H.; Laws, K. Corrosion performance of Ni-based structural alloys for applications in molten-salt based energy systems: Experiment & numerical validation. *Corros. Sci.* **2021**, *190*, 109607. [CrossRef]
124. Karfidov, E.; Nikitina, E.; Erzhenkov, M.; Seliverstov, K.; Chernenky, P.; Mullabaev, A.; Tsvetov, V.; Mushnikov, P.; Karimov, K.; Molchanova, N.; et al. Corrosion Behavior of Candidate Functional Materials for Molten Salts Reactors in LiF–NaF–KF Containing Actinide Fluoride Imitators. *Materials* **2022**, *15*, 761. [CrossRef]
125. Yu, W.; Singh, D.; France, D.M. Investigation of Corrosion of 304 Stainless, Inconel 625, and Haynes 230 in a Chloride-Salt-Based Thermal Storage Medium. *J. Mater. Eng. Perform.* **2019**, *28*, 7379–7389. [CrossRef]
126. Yin, H.; Qiu, J.; Liu, H.; Liu, W.; Wang, Y.; Fei, Z.; Zhao, S.; An, X.; Cheng, J.; Chen, T.; et al. Effect of CrF 3 on the corrosion behaviour of Hastelloy-N and 316L stainless steel alloys in FLiNaK molten salt. *Corros. Sci.* **2018**, *131*, 355–364. [CrossRef]
127. Olson, L.C.; Ambrosek, J.W.; Sridharan, K.; Anderson, M.H.; Allen, T.R. Materials corrosion in molten LiF–NaF–KF salt. *J. Fluor. Chem.* **2009**, *130*, 67–73. [CrossRef]
128. Gomes, A.; Navas, M.; Uranga, N.; Paiva, T.; Figueira, I.; Diamantino, T. High-temperature corrosion performance of austenitic stainless steels type AISI 316L and AISI 321H, in molten Solar Salt. *Sol. Energy* **2018**, *177*, 408–419. [CrossRef]
129. Prieto, C.; Ruiz-Cabañas, F.J.; Madina, V.; Fernández, A.I.; Cabeza, L.F. Corrosion performance of alloy 800H and alloy 625 for potential use as molten salts solar receiver materials in concentrating solar power tower plants. *J. Energy Storage* **2022**, *55*, 105824. [CrossRef]
130. Zhang, X.; Zhang, C.; Wu, Y.; Lu, Y. Experimental research of high temperature dynamic corrosion characteristic of stainless steels in nitrate eutectic molten salt. *JOM* **2020**, *209*, 618–627. [CrossRef]
131. Fernández, A.G.; Cabeza, L.F. Corrosion monitoring and mitigation techniques on advanced thermal energy storage materials for CSP plants. *Sol. Energy Mater. Sol. Cells* **2019**, *192*, 179–187. [CrossRef]
132. Fernández, G.; Pineda, F.; Fuentealba, E.; Jullian, D.; Mallco, A.; Walczak, M. Compatibility of alumina forming alloys with LiNO3-containing molten salts for solar thermal plants. *J. Energy Storage* **2022**, *48*, 103988. [CrossRef]
133. Brito-Hernandez, D.; Lopez-Sesenes, R.; Haro, S.; Porcayo-Calderon, J.; Gonzalez-Rodriguez, J.G. Corrosion behavior of UCX, KHR35, and KHR45 alloys in molten nitrates. *Mater. Corros.* **2020**, *71*, 1783–1793. [CrossRef]
134. Guo, S.; Zhuo, W.; Wang, Y.; Zhang, J. Europium induced alloy corrosion and cracking in molten chloride media for nuclear applications. *Corros. Sci.* **2019**, *163*, 108279. [CrossRef]
135. Cho, S.-H.; Park, S.-B.; Lee, J.-H.; Hur, J.-M.; Lee, H.-S. Cyclic Corrosion Behavior of Ni-Based Superalloys in Hot Lithium Molten Salt. *Oxid. Met.* **2012**, *78*, 153–165. [CrossRef]
136. Bell, S.; Sarvghad, M.; Ong, T.-C.; Naylor, D.; Wang, X.; Yin, Y.; Rumman, R.; Andersson, G.; Will, G.; Lewis, D.A.; et al. Corrosion of iron–nickel–chromium alloys in high temperature carbonate salt under argon atmosphere. *Sol. Energy Mater. Sol. Cells* **2023**, *256*, 112317. [CrossRef]
137. Keny, S.J.; Gupta, V.K.; Kumbhar, A.G.; Rangarajan, S.; Daitkar, M.R.; Maheshwari, N.K.; Vijayan, P.K.; Jagatap, B.N. Corrosion tests of various alloys in fluorides of lithium, sodium and potassium (FLiNaK) medium for molten salt reactors in the temperature range of 550-750oC using electrochemical techniques. *Indian J. Chem. Technol.* **2019**, *26*, 84–88.
138. Kettrakul, P.; Siripongsakul, T.; Promdirek, P. Corrosion behavior of stainless steels in molten salts used for concentrated solar power. *Suranaree J. Sci. Technol.* **2022**, *29*, 1–6.
139. Li, H.; Feng, X.; Wang, X.; Yang, X.; Tang, J.; Gong, J. Impact of temperature on corrosion behavior of austenitic stainless steels in solar salt for CSP application: An electrochemical study. *Sol. Energy Mater. Sol. Cells* **2022**, *239*, 111661. [CrossRef]
140. Nyby, C.; Guo, X.; Saal, J.E.; Chien, S.-C.; Gerard, A.Y.; Ke, H.; Li, T.; Lu, P.; Oberdorfer, C.; Sahu, S.; et al. Electrochemical metrics for corrosion resistant alloys. *Sci. Data* **2021**, *8*, 448–487. [CrossRef] [PubMed]
141. Guo, S.; Zhang, J.; Wu, W.; Zhou, W. Corrosion in the molten fluoride and chloride salts and materials development for nuclear applications. *Prog. Mater. Sci.* **2018**, *97*, 448–487. [CrossRef]

142. Liu, M.; Bell, S.; Segarra, M.; Tay, N.S.; Will, G.; Saman, W.; Bruno, F. A eutectic salt high temperature phase change material: Thermal stability and corrosion of SS316 with respect to thermal cycling. *Sol. Energy Mater. Sol. Cells* **2017**, *170*, 1–7. [CrossRef]
143. Yang, C.; Muránsky, O.; Zhu, H.; Karatchevtseva, I.; Holmes, R.; Avdeev, M.; Jia, Y.; Huang, H.; Zhou, X. Corrosion performance of Ni-16%wt.Mo-X%wt.SiC alloys in FLiNaK molten salt. *Corros. Sci.* **2018**, *143*, 240–248. [CrossRef]
144. Patel, K.; Mahajan, C.; Muskeri, S.; Mukherjee, S. Corrosion Behavior of Refractory High-Entropy Alloys in FLiNaK Molten Salts. *Metals* **2023**, *13*, 450. [CrossRef]
145. Chang, J.; Wang, D.; Zhang, G.; Lou, L.; Zhang, J. Interaction of Ta and Cr on Type-I hot corrosion resistance of single crystal Ni-base superalloys. *JOM* **2017**, *117*, 35–42. [CrossRef]
146. Patel, K.; Hasannaeimi, V.; Sadeghilaridjani, M.; Muskeri, S.; Mahajan, C.; Mukherjee, S. Molten Salt Corrosion Behavior of Dual-Phase High Entropy Alloy for Concentrating Solar Power Systems. *Entropy* **2023**, *25*, 296. [CrossRef]
147. Garip, Y. An investigation on the corrosion performance of $Fe_2CoCrNi0.5$ based high entropy alloys. *Corros. Sci.* **2022**, *206*, 110497. [CrossRef]
148. Cho, S.-H.; Lee, S.-K.; Kim, D.-Y.; Lee, J.-H.; Hur, J.-M. Effects of alloying elements of nickel-based alloys on the hot-corrosion behavior in an electrolytic reduction process. *J. Alloy. Compd.* **2017**, *695*, 2878–2885. [CrossRef]
149. Wan, L.; Zhang, Z.; Wang, W.; Xue, Y.; Shen, J.; Sun, T.; Sun, H. Research on Hot Corrosion Behavior of DZ40M and K452 Superalloys in NaCl Molten Salt. *Materials* **2022**, *15*, 1512. [CrossRef] [PubMed]
150. Zhu, M.; Yi, H.; Lu, J.; Huang, C.; Zhang, H.; Bo, P.; Huang, J. Corrosion of Ni–Fe based alloy in chloride molten salts for concentrating solar power containing aluminum as corrosion inhibitor. *Sol. Energy Mater. Sol. Cells* **2022**, *241*, 111737. [CrossRef]
151. Zhang, T.B.; Dong, R.F.; Hu, R.; Kou, H.C.; Li, J.S. Hot corrosion characteristics of Ni−20Cr−18W superalloy in molten salt. *Trans. Nonferrous Met. Soc. China* **2015**, *25*, 3840–3846. [CrossRef]
152. Chang, J.; Wang, D.; Liu, T.; Zhang, G.; Lou, L.; Zhang, J. Role of tantalum in the hot corrosion of a Ni-base single crystal superalloy. *Corros. Sci.* **2015**, *98*, 585–591. [CrossRef]
153. Li, Y.; Spiegel, M.; Shimada, S. Corrosion behaviour of various model alloys with NaCl–KCl coating. *Mater. Chem. Phys.* **2005**, *93*, 217–223. [CrossRef]
154. Morales, M.; Cabezas, L.; Castro-Alloca, M.; Fargas, G.; Llanes, L.; Mateo, A. Corrosion Evaluation of Austenitic and Duplex Stainless Steels in Molten Carbonate Salts at 600 °C for Thermal Energy Storage. *Metals* **2022**, *12*, 2190. [CrossRef]
155. Zhang, Y.; Xiao, L.; Liu, J. Corrosion behavior of Incoloy 840 in molten nitrate salt for CSP plants. *IOP Conf. Ser. Mater. Sci. Eng.* **2021**, *1167*, 012002. [CrossRef]
156. Hamdy, E.; Strach, M.; Olovsjö, J.N.; Geers, C. Differentiation in corrosion performance of alumina forming alloys in alkali carbonate melts. *Corros. Sci.* **2021**, *192*, 109857. [CrossRef]
157. Dedov, K.V.; Raguzina, E.V.; Abramov, A.V.; Kazakovtseva, E.V.; Zhilyakov, A.Y.; Polovov, I.B.; Volkovich, V.A.; Shak, A.V.; Nikitina, E.V.; Rebrin, O.I. Corrosion Behavior of EP-823 Type Steel in Uranium Containing Chloride Melts. In Proceedings of the VI International Young Researchers' Conference, Ekaterinburg, Russia, 20–23 May 2019; Volume 15, p. 020017.
158. Pavlík, V.; Barborík, P.; Miroslav, M.B.; Vasková, Z. Interaction of metallic zirconium and its alloys Zry-2 and E110 with molten eutectic salt of LiF–NaF–KF containing zirconium fluoride components. *Chem. Pap.* **2016**, *70*, 197–205. [CrossRef]
159. Brito-Hernádez, D.; Rosales-Cadena, I.; Gónzalez-Rodríguez, J.G.; Uruchurtu-Chavarín, J.; Guardían-Tapia, R.; Vera-Dimas, J.G.; López-Sesenes, R. Effect of zirconia in the corrosion behavior of intermetallic Mo_3Si alloy in molten salts mixture of $NaNO_3$ and KNO_3. *Mater. Corros.* **2023**, *74*, 1066–1075. [CrossRef]
160. Amaya, M.; Espinosa-Medina, M.; Porcayo-Calderon, J.; Martinez, L.; Gonzalez-Rodriguez, J. High temperature corrosion performance of FeAl intermetallic alloys in molten salts. *Mater. Sci. Eng. A* **2003**, *349*, 12–19. [CrossRef]
161. Lü, L.; Chen, D.; Ren, X.-L.; Zhang, Q.-M.; Zhang, Y.-C.; Zhou, T. Vital nodes identification in complex networks. *Phys. Rep.* **2016**, *650*, 1–63. [CrossRef]
162. Polovov, I.B.; Abramov, A.V.; Alimgulov, R.R.; Zolotarev, D.A.; Trubcheninova, A.I.; Gibadullina, A.F.; Volkovich, V.A.; Zhilyakov, A.Y.; Khotinov, V.A.; Belikov, S.V. Corrosion of Metallic Materials in the Molten FLiNaK. *ECS Trans.* **2020**, *98*, 453–462. [CrossRef]
163. Alimgulov, R.R.; Trubcheninova, A.I.; Abramov, A.V.; Zhilyakov, A.Y.; Belikov, S.V.; Rebrin, O.I.; Polovov, I.B. Corrosion of Metallic Materials in 3LiCl–2KCl and (3LiCl–2KCl)–UCl3. *ECS Trans.* **2020**, *98*, 307. [CrossRef]
164. Knosalla, C.; Lau, M.; Schmies, L.; Lippmann, W.; Hurtado, A. Investigation on the Corrosion Behavior of Nickel-Base Alloys in Molten Chlorides for Sensible Heat Energy Applications. *Adv. Eng. Mater.* **2020**, *22*, 2000099. [CrossRef]
165. Ouyang, F.-Y.; Chang, C.-H.; Kai, J.-J. Long-term corrosion behaviors of Hastelloy-N and Hastelloy-B3 in moisture-containing molten FLiNaK salt environments. *J. Nucl. Mater.* **2014**, *446*, 81–89. [CrossRef]
166. Ouyang, F.-Y.; Chang, C.-H.; You, B.-C.; Yeh, T.-K.; Kai, J.-J. Effect of moisture on corrosion of Ni-based alloys in molten alkali fluoride FLiNaK salt environments. *J. Nucl. Mater.* **2013**, *437*, 201–207. [CrossRef]
167. Sun, H.; Zhang, P.; Wang, J. Effects of alloying elements on the corrosion behavior of Ni-based alloys in molten NaCl-KCl-$MgCl_2$ salt at different temperatures. *Corros. Sci.* **2018**, *143*, 187–199. [CrossRef]
168. Sun, H.; Wang, J.Q.; Tang, Z.; Liu, Y.; Wang, C. Assessment of effects of Mg treatment on corrosivity of molten NaCl-KCl-$MgCl_2$ salt with Raman and Infrared spectra. *Corros. Sci.* **2020**, *164*, 108350. [CrossRef]
169. Sankar, K.M.; Singh, P.M. Effect of oxide impurities on the corrosion behavior of structural materials in molten LiF-NaF-KF. *Corros. Sci.* **2022**, *206*, 110473. [CrossRef]

170. Abramov, A.V.; Karpov, V.V.; Zhilyakov, A.Y.; Gibadullina, A.F.; Polovov, I.B.; Volkovich, V.A.; Belikov, S.V.; Shak, A.V.; Rebrin, O.I. Corrosion of Corrosion-Resistant and High-Temperature Nickel-Based Alloys in Chloroaluminate Melts. *ECS Trans.* **2014**, *64*, 217. [CrossRef]
171. Karpov, V.V.; Bazhenov, A.V.; Abramov, A.V.; Rebrin, O.I. Corrosion resistance of alloys of Hastelloy in chloroaluminate melts. *Chim. Techno Acta* **2015**, *2*, 131–138. [CrossRef]
172. Slusser, J.W.; Titcomb, J.B.; Heffelfinger, M.T.; Dunbobbin, B.R. Corrosion in Molten Nitrate-Nitrite Salts. *JOM* **1985**, *37*, 24–27. [CrossRef]
173. Park, S.K.; Lee, T.H.; Sim, M.S.; Noh, J.S.; Cho, S.H.; Lee, J.H. Alloy Design of New Ni-Based Structural Materials for Electrolytic Reduction and its Corrosion Behavior in Lithium Molten Salt. *Adv. Mater. Res.* **2014**, *886*, 41–44. [CrossRef]
174. Jalbuena, A.A.; Ury, N.; Bae, J.; Faraj, C.; Hanan, K.; Kasnakjian, S.; Logier, J.K.; Mishra, R.S.; Wang, X.; Earthman, J.C.; et al. Corrosion of $Al_{0.1}$CoCrFeNi High Entropy Alloy in a Molten Eutectic Salt. *J. Electrochem. Soc.* **2019**, *166*, C3488–C3492. [CrossRef]
175. Liu, S.; Wang, R.; Wang, L.; Ge, F.; Gao, M.; Si, Y.; Li, B. Corrosion behavior of iron-based and Ni-based alloys melted in NaCl–$MgCl_2$–KCl mixed molten salt under vacuum atmosphere. *J. Mater. Res. Technol.* **2023**, *28*, 1915–1923. [CrossRef]
176. Gomez-Vidal, J.; Fernandez, A.; Tirawat, R.; Turchi, C.; Huddleston, W. Corrosion resistance of alumina-forming alloys against molten chlorides for energy production. I: Pre-oxidation treatment and isothermal corrosion tests. *Sol. Energy Mater. Sol. Cells* **2017**, *166*, 222–233. [CrossRef]
177. Song, Y.; Shen, M.; Peng, H.; Wang, C.; Zhao, S.; Zuo, Y.; Xie, L. Solubility of Cr_2O_3 in Molten Fluorides with Different ZrF4 Contents and Fluoroacidities. *J. Electrochem. Soc.* **2020**, *167*, 023501. [CrossRef]
178. Ishitsuka, T.; Nose, K. Stability of protective oxide films in waste incineration environment—Solubility measurement of oxides in molten chlorides. *Corros. Sci.* **2002**, *44*, 247–263. [CrossRef]
179. Atamert, S. Stability, Wear Resistance and Microstructure of Iron, Nickel-Based Alloys. Ph.D. Thesis, University of Cambridge, Cambridge, UK, 1988.
180. Aubry, P.; Blanc, C.; Demirci, I.; Gorny, C.; Maskrot, H. Analysis of a Ni-Fe-Cr-Mo-Si hardfacing alloy manufactured by laser cladding: Influence of the iron content on the wear resistance properties. *Procedia CIRP* **2018**, *74*, 210–213. [CrossRef]
181. Yoo, J.W.; Lee, S.H.; Yoon, C.S.; Kim, S.J. The effect of boron on the wear behavior of iron-based hardfacing alloys for nuclear power plants valves. *J. Nucl. Mater.* **2006**, *352*, 90–96. [CrossRef]
182. Liu, R.; Yao, M.X.; Patnaik, P.C.; Wu, X. Effects of Heat Treatment on Mechanical and Tribological Properties of Cobalt-Base Tribaloy Alloys. *J. Mater. Eng. Perform.* **2005**, *14*, 634–640. [CrossRef]
183. Zhang, H.; Shi, Y.; Kutsuna, M.; Xu, G. Laser cladding of Colmonoy 6 powder on AISI316L austenitic stainless steel. *Nucl. Eng. Des.* **2010**, *240*, 2691–2696. [CrossRef]
184. Kashani, H.; Amadeh, A.; Ghasemi, H. Room and high temperature wear behaviors of nickel and cobalt base weld overlay coatings on hot forging dies. *Wear* **2006**, *262*, 800–806. [CrossRef]
185. Bregliozzi, G.; Di Schino, A.; Kenny, J.; Haefke, H. The influence of atmospheric humidity and grain size on the friction and wear of AISI 304 austenitic stainless steel. *Mater. Lett.* **2003**, *57*, 4505–4508. [CrossRef]
186. Rendón, J.; Olsson, M. Abrasive wear resistance of some commercial abrasion resistant steels evaluated by laboratory test methods. *Wear* **2009**, *267*, 2055–2061. [CrossRef]
187. Ding, Y.; Liu, R.; Yao, J.; Zhang, Q.; Wang, L. Stellite alloy mixture hardfacing via laser cladding for control valve seat sealing surfaces. *Surf. Coatings Technol.* **2017**, *329*, 97–108. [CrossRef]
188. Singh, J.; Kumar, S.; Mohapatra, S. Erosion tribo-performance of HVOF deposited Stellite-6 and Colmonoy-88 micron layers on SS-316L. *Tribol. Int.* **2018**, *147*, 105262. [CrossRef]
189. Vikstroem, J. Galling Resistance of Hardfacing Alloys Replacing Stellite. *Wear* **1994**, *179*, 143–146. [CrossRef]
190. Ocken, H. *Performance of NOREM (TM) Hardfacing Alloys*; Report No.: TR-112993; Palo Alto, CA, USA, 1999; Available online: https://www.epri.com/research/products/TR-112993 (accessed on 29 October 2024).
191. Cockeram, B.V.; Buck, R.F.; Wilson, W.L. Laboratory galling tests of several commercial cobalt-free weld hardfacing alloys. *Surf. Coat. Technol.* **1997**, *94*, 495–500. [CrossRef]
192. Wu, W.; Wu, L.-T. The wear behavior between hardfacing materials. *Met. Mater. Trans. A* **1996**, *27*, 3639–3648. [CrossRef]
193. Coelho, L.B.; Zhang, D.; Van Ingelgem, Y.; Steckelmacher, D.; Nowé, A.; Terryn, H. Reviewing machine learning of corrosion prediction in a data-oriented perspective. *Npj Mater. Degrad.* **2022**, *6*, 8. [CrossRef]
194. Papadimitriou, I.; Gialampoukidis, I.; Vrochidis, S.; Kompatsiaris, I. AI methods in materials design, discovery and manufacturing: A review. *Comput. Mater. Sci.* **2024**, *235*, 112793. [CrossRef]
195. Li, X.; Zhang, D.; Liu, Z.; Li, Z.; Du, C.; Dong, C. Materials science: Share corrosion data. *Nature* **2015**, *527*, 441–442. [CrossRef]